

# A Study of the Korg MS10 & MS20 Filters

Timothy E. Stinchcombe <sup>†</sup>

30 August 2006 <sup>‡</sup>

---

<sup>†</sup>Comments, suggestions and corrections can be emailed to me at:

`tim102@tstinchcombe.freemove.co.uk`.

A good place to seek answers to questions on the internals of synthesizers in general is the ‘Synth DIY’ mailing list: <http://dropmix.xs4all.nl/synth-diy/>

<sup>‡</sup>Corrections to links and minor typos, 13 Dec 2009



## Contents

<b>1</b>	<b>Introduction</b>	<b>4</b>
<b>2</b>	<b>Filter Schematics, Structures and Transfer Functions</b>	<b>5</b>
2.1	Transfer function of the OTA version . . . . .	8
2.2	Transfer function of the Korg35 version . . . . .	10
<b>3</b>	<b>Korg35 Voltage Control of the Cut-Off Frequency</b>	<b>13</b>
3.1	Reverse saturation mode . . . . .	13
3.2	Exponential control . . . . .	20
<b>4</b>	<b>Asymmetrical Frequency and Resonance Responses of the Korg35</b>	<b>29</b>
<b>5</b>	<b>Non-Linear Effects of the Feedback Diodes</b>	<b>30</b>
<b>6</b>	<b>Exponential Control in the OTA Version</b>	<b>36</b>
<b>7</b>	<b>The High-Pass Filter Variants are 6dB, not 12!</b>	<b>39</b>
<b>8</b>	<b>Sallen-Key ‘Myths’ Discredited</b>	<b>40</b>
<b>9</b>	<b>Conclusion</b>	<b>43</b>
<b>10</b>	<b>Acknowledgements, Rights and Copyrights</b>	<b>45</b>
	<b>References</b>	<b>46</b>

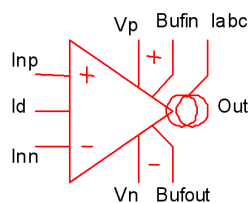
## 1 Introduction

This paper contains a reasonably thorough analysis of the filters used in the Korg MS10 and MS20, concentrating for the most part on the low-pass variants of those filters. The filters have a reputation for having lots of ‘character’, and if we attempt to attribute this to some facet of the filters’ topology, we immediately run into much confusion: filters in the MS10 and early MS20s were built around a Korg-proprietary, resin-sealed device, the ‘Korg35’; in later MS20s, the filter was re-designed around the LM13600 operational transconductance amplifier (OTA). Korg finally divulged the circuitry inside the Korg35 in 2000, confirming that the filters’ topology was indeed one of the standard Sallen-Key types, as had been suspected for some time; the later OTA-based filter however is basically two cascaded, buffered first-order sections, which whilst still being a second-order filter, does not share the same Sallen-Key topology of the original.

There are several purposes to my study. Firstly there is the mechanism by which the transistors in the Korg35 chip are used to provide voltage-control of the filter cut-off frequency: barring simple substitution of vactrols for resistors, adding voltage-control to a standard filter topology such as the Sallen-Key types may require a good deal of ingenuity. Korg have demonstrated such ingenuity by biasing two transistors in the Korg35 in the *reverse* saturation mode, thus essentially using them as current-controlled resistors, and I was keen to better understand how on earth this works.

Secondly, when mention is made of the MS20 filter and its “legendary sound”, it is often unclear just *which* of the two filter types is being referred to: do they have such similar aural characteristics that it is immaterial which one is actually meant? It will be shown in this paper that, analytically at least, the two filter designs have similarities, but there are also differences, and these are shown too. Ultimately the best test of their similarity/difference will be to listen to actual hardware: this will form the next phase in my study, that of building copies of both types of filter.

**Schematics and simulation:** all schematics in this document have been produced in SIMetrix, [11], a SPICE-type simulation package. Where possible I have used ‘recognized’ models for the Japanese transistors: I was unable to find one for the 2SK94 JFET, and so have used a BF245A instead, as it has a similar threshold voltage range. I have generated my own OTA symbol, whose pin-outs are



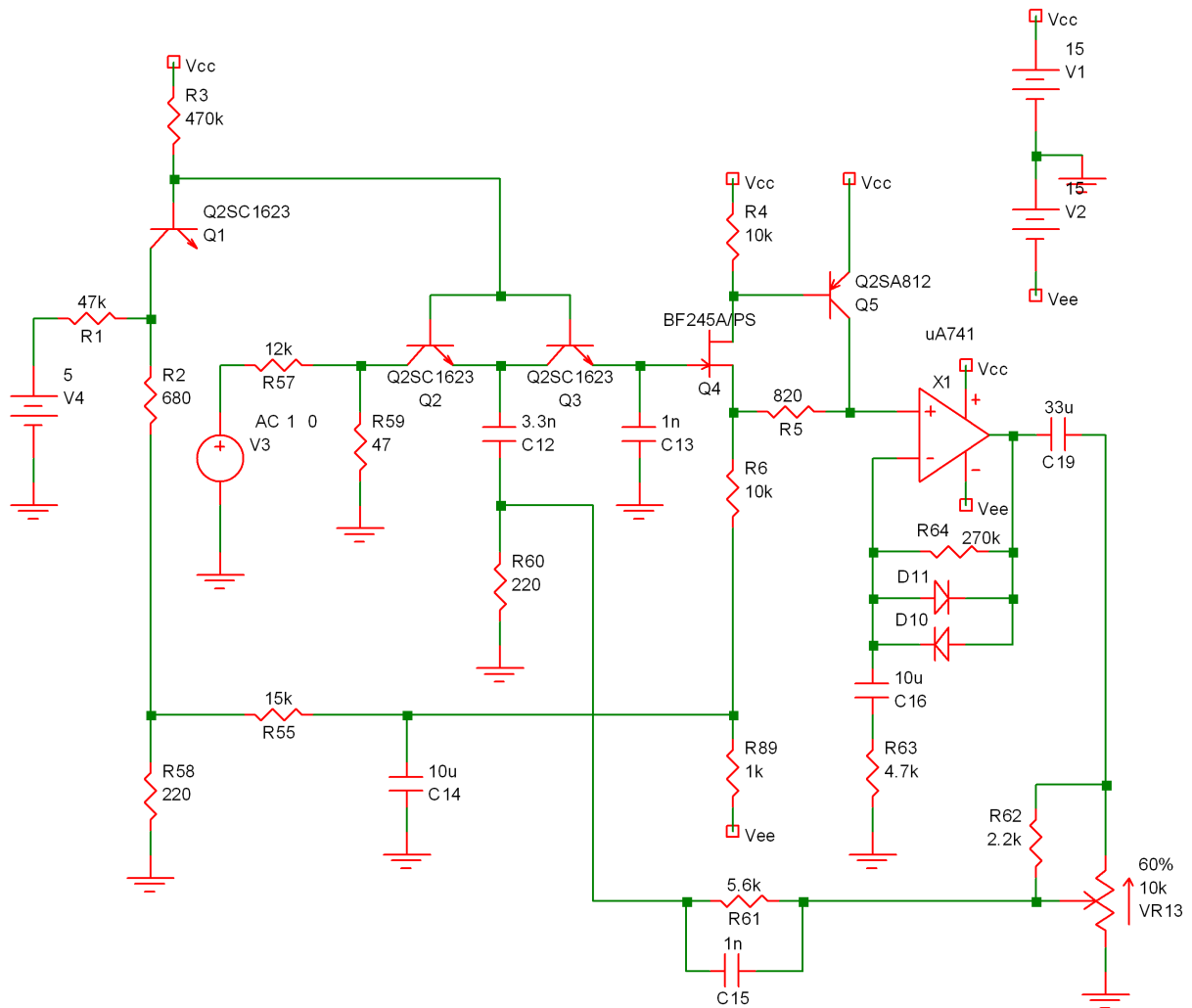


Figure 1: MS10 version of the Korg35-based filter

as when I imported the National LM13600/13700 models, the symbol SIMetrix assigned was a bit ‘generic’.

## 2 Filter Schematics, Structures and Transfer Functions

Figures 1 and 2 are schematics for the two filter types: the earlier Korg35-based one in the former, and the later OTA-based filter in the latter. The Korg35-based schematic takes the MS10 component values, mainly for the simple expedient that the copy of the MS10 schematic I found on the web was easier to read than that which I found for the MS20. I’ve not yet seen either an MS10 or MS20 in the flesh, but it seems the later OTA-based filter was constructed around a ‘daughterboard’ PCB, the ‘KLM-307’, for which I also found a readable schematic. In both figures I have tried to keep the nomenclature of the discrete components as the original schematics, for ease of

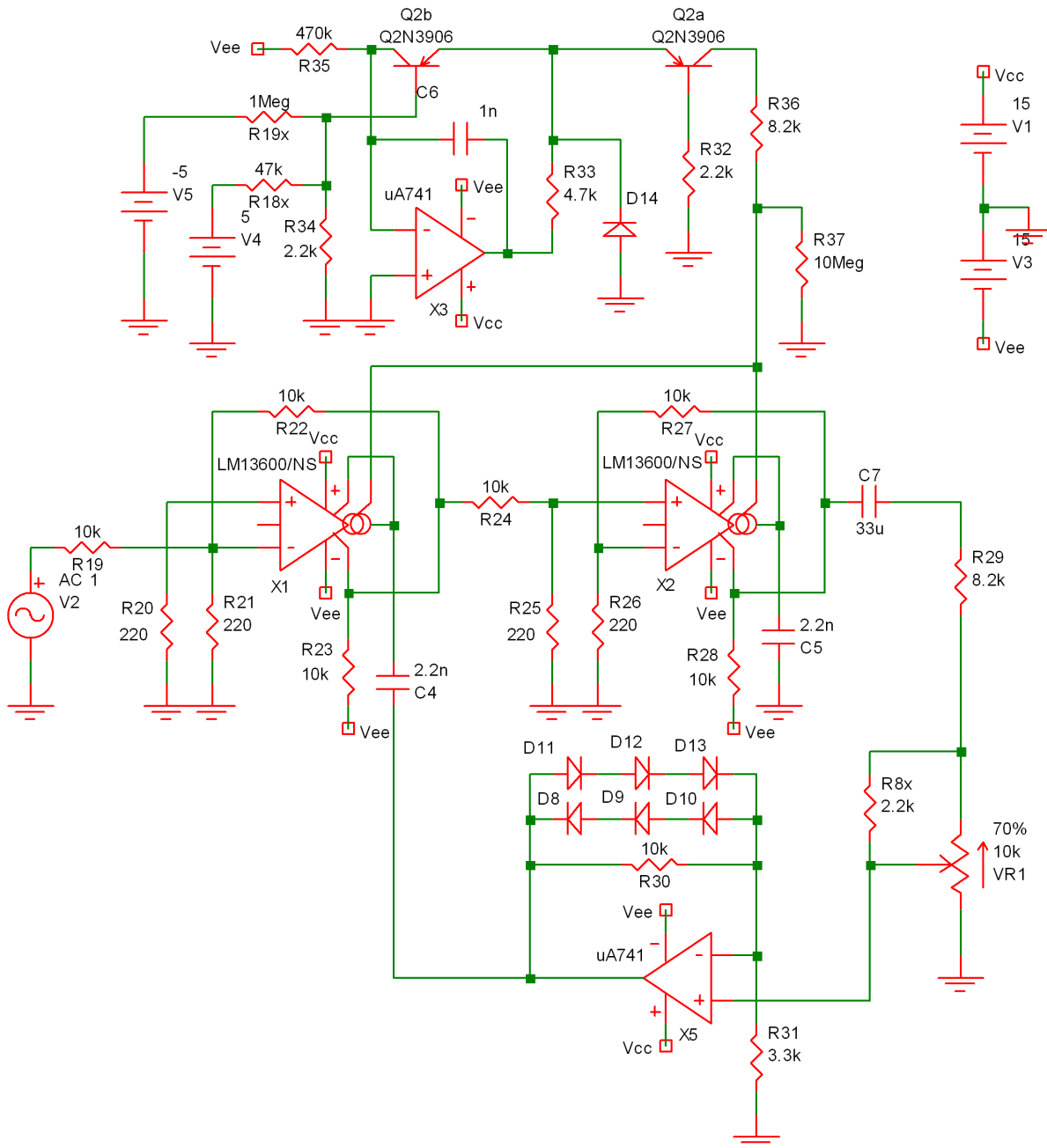


Figure 2: OTA-based version of later MS20s

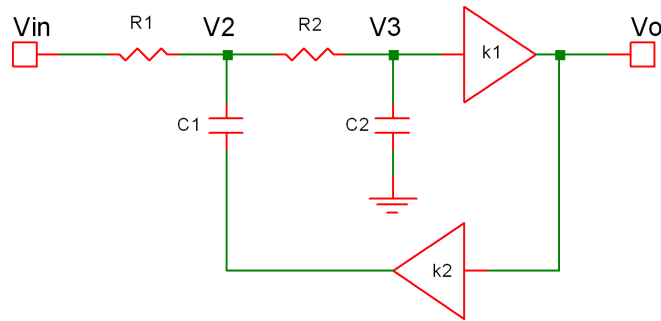


Figure 3: Sallen-Key low-pass structure of the Korg35-based filter

reference.

In Figure 1:  $V_3$  is the input voltage;  $V_4$  the cut-off frequency control voltage; the output is taken at  $C_{19}/R_{62}$ ;  $VR_{13}$  is the resonance control pot. In Figure 2:  $V_2$  is the input;  $V_4$  the cut-off voltage ( $V_5$  is an offset-adjustment for the cut-off); the output is  $C_7/R_{29}$ ;  $VR_1$  is the resonance pot.

One of the most obvious differences between the two filter types is that the non-linearity-producing diodes in the early filter is in the forward path, whilst in the OTA version they are in the feedback loop. If we ignore these diodes for the moment (they are covered in detail in Section 5 later), and disregard the cut-off frequency control circuitry, then the basic structure of the Korg35-based filter is as in Figure 3: here resistors  $R_1$  and  $R_2$  are actually formed by  $Q_2$  and  $Q_3$  in the real thing, which are acting as current-controlled resistors; gain block  $k_1$  is formed from the JFET buffer and the non-inverting op amp set-up around  $X_1$ ; gain  $k_2$  consists of  $VR_{13}/R_{62}$  and potential divider  $R_{61}/R_{60}$ . This is easily recognizable as the main low-pass filter topology of the Sallen-Key family of filters, [3].

The basic structure of the OTA-based filter is shown in Figure 4, which is slightly harder to see due to the use of the OTAs and supporting circuitry (more on this in a moment). In the figure:  $R_1$  and  $R_2$  represent the variable-resistor roles performed by the OTAs ( $X_1$  and  $X_2$ ); gain  $k_1$  is basically the (unity gain) buffer at  $X_2$  OTA's output; gain  $k_2$  is  $R_{8x}/VR_1$  and non-inverting op amp set-up  $X_5$ . The noteworthy difference with Figure 3 is the inclusion of the unity gain buffer at the output of the first OTA ( $X_1$ ): this means that there is no loading effect of the second filter stage upon the first, as there is in the Sallen-Key set-up. The effect on the derivation of the transfer function is not great, as we'll see below, but I do not believe this set-up corresponds to any of those in [3], and so therefore I do not regard it as being a Sallen-Key filter.

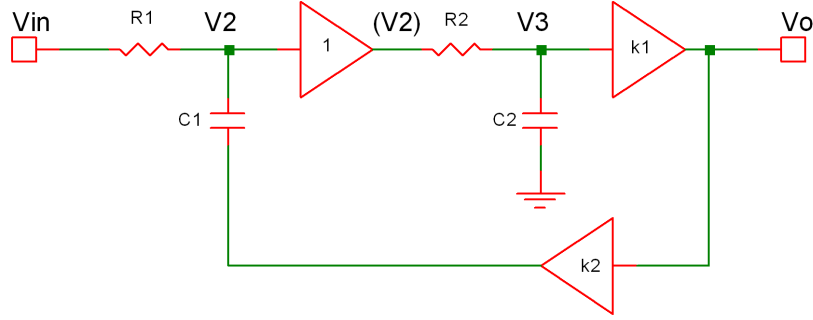
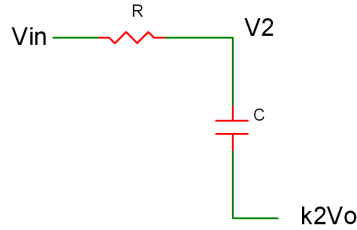


Figure 4: Basic filter structure of the OTA version

## 2.1 Transfer function of the OTA version

The equivalence of the OTA set-ups to simple  $RC$  sections is not immediately obvious to me. Whether with sufficient intuition and familiarity with OTAs it is possible to quickly establish what such a circuit does, or simply with enough exposure one merely *recognizes* what it is, I do not know, and in any case with my limited electronics experience I do not possess the ability to do either: thus I shall do what many do when faced with apparently such a complex situation—resort to some mathematics! ([9].)

Consider the following simple situation:



and we require an expression for  $V_2$  in terms of  $V_{in}$  and  $V_o$ . By nodal analysis (current in = current out) at the  $V_2$  node, we get

$$\frac{V_{in}}{R} + k_2 V_o s C = \frac{V_2}{R} + V_2 s C, \quad (1)$$

then

$$V_{in} + k_2 V_o s C R = V_2 + V_2 s C R,$$

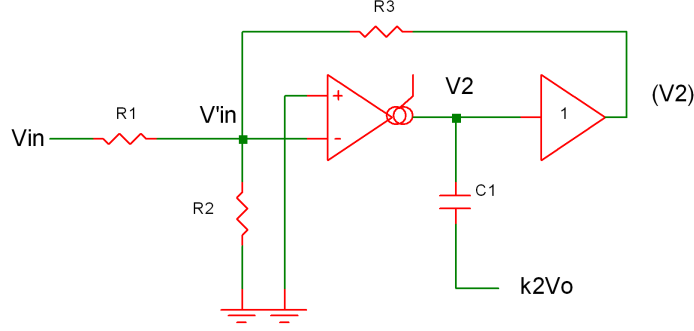
which easily leads to

$$V_2 \left( 1 + \frac{s}{\omega_c} \right) = V_{in} + k_2 V_o \frac{s}{\omega_c} \quad (2)$$

on putting  $\omega_c = 1/RC$ . If  $C$  were grounded, i.e.  $V_o = 0$ , this gives the familiar first order low-pass transfer function

$$\frac{V_2}{V_{in}} = \frac{1}{\left( 1 + \frac{s}{\omega_c} \right)}.$$

Now consider this diagrammatic representation of the first OTA stage:



Nodal analysis at the  $V'_{in}$  node gives

$$\frac{V_{in}}{R_1} + \frac{V_2}{R_3} = V'_{in} \left( \frac{1}{R_1} + \frac{1}{R_2} + \frac{1}{R_3} \right),$$

and for  $R_1 = R_3$

$$V_{in} + V_2 = V'_{in} \left( 2 + \frac{R_1}{R_2} \right),$$

which further simplifies to

$$V'_{in} = k(V_{in} + V_2)$$

where  $k \approx R_2/R_1$  when  $R_1 \gg R_2$ , which is usually the case. From the standard expression for an OTA (for example [10]), and with  $i_o$  the current output from the OTA, we have

$$\begin{aligned} i_o &= 19.2I_{abc}(V_+ - V_-) \\ &= -Kk(V_{in} + V_2) \end{aligned}$$

writing  $K = 19.2I_{abc}$ , carefully noting that gain  $K$  is variable, depending on the 'amplifier bias current',  $I_{abc}$ . On the assumption that the OTA's output buffer doesn't take any current, then all of  $i_o$  goes through  $C_1$ , so

$$i_o = (V_2 - k_2V_o)sC_1.$$

Equating these two expressions gives

$$-Kk(V_{in} + V_2) = (V_2 - k_2V_o)sC_1$$

which arranges to

$$V_2(Kk + sC_1) = -KkV_{in} + k_2V_0sC_1$$

then

$$V_2 \left( 1 + \frac{s}{\omega_c} \right) = -V_{in} + k_2V_0 \frac{s}{\omega_c}, \quad (3)$$

where this time we have put  $\omega_c = Kk/C_1$ . Apart from the negation of  $V_{in}$  (which is easy to see is due to applying  $V_{in}$  to the OTA's inverting input), this is identical to equation (2) above. Thus the OTA set-up *is* equivalent to a simple  $RC$  section, with the benefit of being able to control the  $R$  using the OTA (through  $I_{abc}$  and hence  $K$ , ultimately affecting the cut-off frequency  $\omega_c$ ).

To complete the transfer function of the OTA version, consider the second OTA stage: from both Figures 2 and 4, we see there is no inversion of ' $V_2$ ' at the OTA input, and no ' $k_2V_o$ ' feedback contribution, so from similarity with equation (3) we get

$$V_3 \left( 1 + \frac{s}{\omega_c} \right) = V_2, \quad (4)$$

or

$$\frac{V_o}{k_1} \left( 1 + \frac{s}{\omega_c} \right) = V_2,$$

as  $V_o = k_1V_3$ , and we have also implicitly made  $C_2 = C_1$ , we are assuming both  $I_{abc}$ 's are equal and that both factors ' $k$ ' are the same, so  $\omega_c = Kk/C_1 = Kk/C_2$ . Substitute for  $V_2$  in (3) above

$$\frac{V_o}{k_1} \left( 1 + \frac{s}{\omega_c} \right) \left( 1 + \frac{s}{\omega_c} \right) = -V_{in} + k_2V_o \frac{s}{\omega_c},$$

and multiply out to get the complete transfer function

$$\frac{V_o}{V_{in}} = \frac{-k_1}{\frac{s^2}{\omega_c^2} + (2 - k_1k_2)\frac{s}{\omega_c} + 1}. \quad (5)$$

In the actual circuit, gain  $k_1$  is just that from the buffer at the second OTA output, so is 1. Gain  $k_2$  is the attenuation from the potential divider action of  $R_{29}$  and pot  $VR_1$ , times the gain of non-inverting op amp in the feedback loop (again noting the fact that for now we are ignoring the diodes): in the real circuit  $R_{31}$  is  $2.2\text{k}\Omega$ , plus a  $2.2\text{k}\Omega$  preset (annotated  $VR_2$  on the KLM-307 schematics), so taking a mid-way value of  $3\text{k}3\Omega$  for  $R_{31}$  as shown in Figure 2, the op amp gain is  $(1 + 10/3.3) \approx 4$ . The pot output is zero at minimum, up to  $10/(8.2 + 10) = 1/1.82$  at its maximum, so overall  $k_2$  is 0 to  $4/1.82=2.2$ , which should be plenty to get it to oscillate. (Indeed this suggests the method of adjusting the preset may have been to turn the resonance to maximum, and then adjust the preset so that the filter is comfortably oscillating.)

## 2.2 Transfer function of the Korg35 version

I ran into something of a pedagogical problem here: I wanted to derive the standard Sallen-Key transfer function in such a way that the differences from the function derived above are highlighted, and at the same time basically followed the same method to show

the similarities, but that it retained the more general case of different  $R$ 's and  $C$ 's (as there is a point to be made on this below), and yet didn't require flogging through a *third* derivation from scratch! What follows isn't particularly elegant, but hopefully gets the job done.

The Sallen-Key filter differs from the OTA-based filter above in that the second stage loads the first: in order to see the effect this has on the final transfer function, track the extra terms through the algebra by annotating them with a '•'. Thus nodal analysis at the  $V_2$  node of Figure 3, cf equation (1), gives:

$$\frac{V_{in}}{R_1} + \frac{V_3^\bullet}{R_2} + k_2 V_o s C_1 = V_2 \left( \frac{1}{R_1} + \frac{1^\bullet}{R_2} + s C_1 \right).$$

Multiplying throughout by  $R_1$ , putting  $\omega_{c1} = 1/R_1 C_1$ , and using  $V_o = k_1 V_3$  then gives

$$V_{in} + \frac{V_o R_1^\bullet}{k_1 R_2} + k_2 V_o \frac{s}{\omega_{c1}} = V_2 \left( 1 + \frac{R_1^\bullet}{R_2} + \frac{s}{\omega_{c1}} \right).$$

The second stage has the same expression as (4) above:

$$V_2 = V_3 \left( 1 + \frac{s}{\omega_{c2}} \right) = \frac{V_o}{k_1} \left( 1 + \frac{s}{\omega_{c2}} \right),$$

but where now  $\omega_{c2} = 1/R_2 C_2$ . Substituting for  $V_2$  in the previous expression gives

$$V_{in} + \frac{V_o R_1^\bullet}{k_1 R_2} + k_2 V_o \frac{s}{\omega_{c1}} = \frac{V_o}{k_1} \left( 1 + \frac{s}{\omega_{c2}} \right) \left( 1 + \frac{R_1^\bullet}{R_2} + \frac{s}{\omega_{c1}} \right),$$

which when multiplied out and re-arranged gives the (rather clumsy) transfer function

$$\frac{V_o}{V_{in}} = \frac{k_1}{\frac{s^2}{\omega_{c1}\omega_{c2}} + \left( (1 - k_1 k_2) \frac{1}{\omega_{c1}} + \left( 1 + \frac{R_1^\bullet}{R_2} \right) \frac{1}{\omega_{c2}} \right) s + 1}. \quad (6)$$

For comparison with the OTA-based transfer function, (5), above, putting  $R_1 = R_2$  and  $C_1 = C_2$ , so  $\omega_{c1} = \omega_{c2} = \omega_c$ , gives the normal Sallen-Key transfer function:

$$\begin{aligned} \frac{V_o}{V_{in}} &= \frac{k_1}{\frac{s^2}{\omega_c^2} + (2 + 1^\bullet - k_1 k_2) \frac{s}{\omega_c} + 1} \\ &= \frac{k_1}{\frac{s^2}{\omega_c^2} + (3 - k_1 k_2) \frac{s}{\omega_c} + 1}, \end{aligned} \quad (7)$$

where the 'bullet' term due to the loading just contributes the extra '1' in the denominator.

An immediate distinction comparing with equation (5) is that this filter would require greater gain around the loop to sustain self-oscillation, i.e.  $k_1 k_2$  needs to be 3, rather than merely 2. From Figure 1,  $k_1$  is the gain of the JFET buffer times

the following non-inverting op amp set-up: simple simulation shows that the former is basically a unity-gain buffer, whilst the second has gain  $1 + 270/4.7 = 58.4$ . Gain  $k_2$  has a maximum value defined by the potential divider  $R_{60}/R_{61}$ , which is  $220/(5600+220) = 1/26.5$ , but is varied from zero up to this value by the resonance potentiometer,  $VR_{13}$ . Thus the maximum value of  $k_1k_2$  is  $58.4/26.5 = 2.2$ : even allowing for the fact that the JFET buffer is probably more like  $1.1\times$  than unity, this still does not make the 3 value required for self-oscillation. This discrepancy of course arises from the fact that the Korg35-based filter doesn't have equal  $R$ 's and  $C$ 's. We do actually have  $C_1 = 3 \times C_2$ , but the case for the  $R$ 's is not so clear (we return to this in Section 3.2 later): however if we assume that  $C_1 = 3 \times C_2$  is deliberately chosen to maintain equal cut-off frequencies of the two sections *because* the equivalent resistances of the transistors  $Q_2$  and  $Q_3$  appear to give  $R_1 \approx R_2/3$ , then the transfer function changes in the right direction. With these values we get

$$\omega_{c2} = \frac{1}{R_2C_2} = \frac{1}{3R_1 \times \frac{C_1}{3}} = \frac{1}{R_1C_1} = \omega_{c1} = \omega_c, \quad \text{say,}$$

and substituting back into equation (6) gives

$$\begin{aligned} \frac{V_o}{V_{in}} &= \frac{k_1}{\frac{s^2}{\omega_c^2} + \left(1 - k_1k_2 + 1 + \frac{1}{3}\right) \frac{s}{\omega_c} + 1} \\ &= \frac{k_1}{\frac{s^2}{\omega_c^2} + \left(2\frac{1}{3} - k_1k_2\right) \frac{s}{\omega_c} + 1}. \end{aligned} \quad (8)$$

This is now much closer to the OTA-based transfer function, equation (5), and it is also clear that self-oscillation is *very* likely to be possible.

Part of my purpose in this study was to investigate whether the differences I perceived between the filter topologies have any impact on the sound of the filters. Most accounts suggest that the two different versions of the MS10/MS20 filters sound quite similar, and even though I have little idea as to how much effect any particular filter's transfer function may have on its sound, the closeness of the transfer functions shown here doesn't seem to run contrary to these accounts. In a similar vein, I am not sure whether plotting the poles yields any useful information: there is a small difference which we'll quickly look at, but I don't know how significant it may be.

Normalize the transfer functions by essentially setting  $\omega_c = 1$ , and take the denominator to be

$$s^2 + (a - k_1k_2)s + 1,$$

where  $a = 2$  for the OTA version, and  $a = 2\frac{1}{3}$  for the Korg35 version. Assuming gains  $k_1k_2$  can be varied from 0 to  $a$  so as to just give oscillation, then write this as

$$s^2 + a(1 - k_r)s + 1,$$

where  $k_r = 0 \rightarrow 1$  is the resonance setting from min to max. Then the filter poles are the roots of this quadratic, which are real when

$$a^2(1 - k_r)^2 \geq 4$$

that is when

$$k_r \leq 1 - \frac{2}{a},$$

and conversely are complex when

$$k_r > 1 - \frac{2}{a}.$$

Since  $k_r \geq 0$ , for real roots the first relation requires

$$1 - \frac{2}{a} \geq k_r \geq 0$$

that is

$$1 - \frac{2}{a} \geq 0,$$

so requiring

$$a \geq 2.$$

Thus for the Korg35 version, where  $a = 2\frac{1}{3}$ , then  $1 - 2/a = 0.143$ : so for  $0 \leq k_r < 0.143$  the poles are real, and paired on the real axis; for  $k_r = 0.143$  the poles coincide at  $(-1, 0)$ ; for  $0.143 < k_r \leq 1$  they are complex conjugate pairs, lying on the unit circle. These are shown in Figure 5, for  $k_r = 0, 0.1, 0.143, 0.25, 0.5, 0.75, 1$  and  $1.1$ .

For the OTA version, since  $a = 2$ , then the only real poles are those coincident at  $(-1, 0)$  when  $k_r = 0$ : thus there is no region where there are poles paired on the real axis—(for any  $k_r > 0$ ) they are all complex conjugate pairs on the unit circle. This difference of course is also reflected in the differing responses as the resonance changes, but all plots of these that I have made do not show any difference worthy of mention.

### 3 Korg35 Voltage Control of the Cut-Off Frequency

#### 3.1 Reverse saturation mode

In the Korg35-based filter, the two resistors of the Sallen-Key filter topology are realized by two of the transistors in the Korg35 chip, which are used as variable resistors. This is achieved by operating the transistors in the ‘reverse saturation mode’, and their equivalent resistance is roughly proportional to their base currents, which are

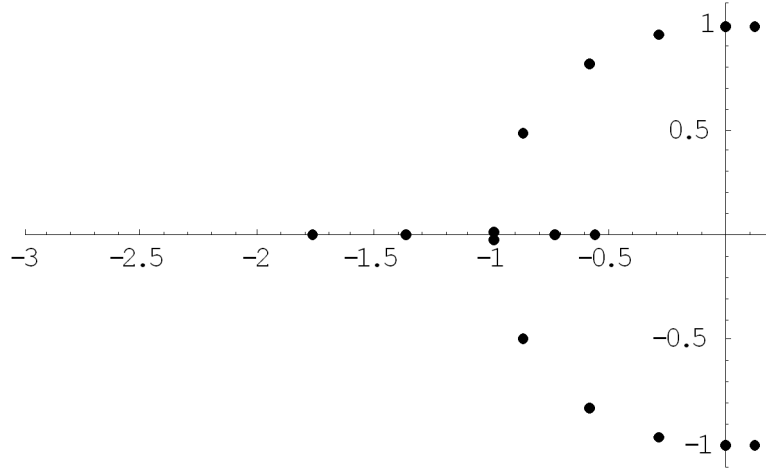


Figure 5: Poles of the (normalized) Korg35 transfer function, equation (8).

supplied via the effect of a third transistor in the chip (and which gives the exponential relationship for the cut-off frequency, to be examined in section 3.2).

In a bipolar junction transistor (BJT), if we swap the collector and emitter we will still have ‘nnp’ or ‘pnp’, so we will still get some transistor action, albeit nowhere near as good as normal since all the fabrication geometries and doping levels are optimized for the forward mode of operation. As they can be when operated in the forward mode, BJTs operated in the reverse mode can also become saturated, and it is in this mode that the transistors in the Korg35 chip are biased. Deriving an expression for the reverse saturation voltage is a little tedious: one is given in [5], equation (4.115) of section 4.13, but as is often the case, quite a lot of detail has been left out. To convince myself of its validity, and so that I got a better grasp of it myself, I worked through some of the detail, which I am including here. However I shall not be giving a detailed description of the Ebers-Moll model, which is adequately covered in [5] and many other places. Notation in the sequel follows that in [5], section 4.13.

The Ebers-Moll model for the BJT represents it as two back-to-back diodes and two current sources, as shown for an npn transistor in Figure 6. The diode currents are

$$i_{DE} = I_{SE}(e^{v_{BE}/V_T} - 1) \quad (9)$$

$$i_{DC} = I_{SC}(e^{v_{BC}/V_T} - 1) \quad (10)$$

where  $V_T$  is the thermal voltage, and  $I_{SE}$  and  $I_{SC}$  are the saturation currents of the diodes. From the figure, the currents can be written as

$$i_E = i_{DE} - \alpha_R i_{DC} \quad (11)$$

$$i_C = -i_{DC} + \alpha_F i_{DE} \quad (12)$$

$$i_B = (1 - \alpha_F) i_{DE} + (1 - \alpha_R) i_{DC} \quad (13)$$

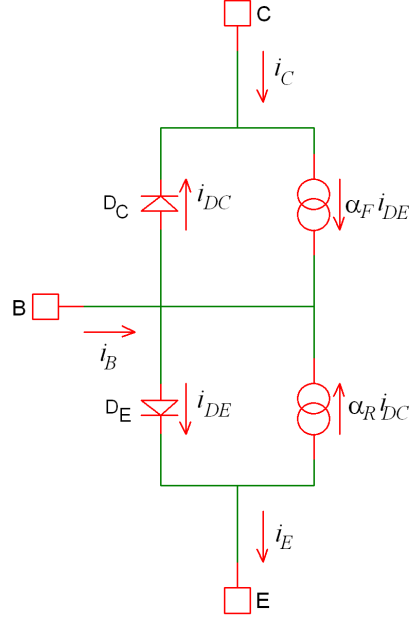


Figure 6: Ebers-Moll model for an npn transistor.

where  $\alpha_F$  ( $\alpha_R$ ) is the forward (reverse) common-base current gain. The saturation currents are related as

$$\alpha_F I_{SE} = \alpha_R I_{SC} = I_S,$$

and using this and substituting for  $i_{DE}$  and  $i_{DC}$  from (9) and (10), (11), (12) and (13) become

$$i_E = \frac{I_S}{\alpha_F} (e^{v_{BE}/V_T} - 1) - I_S (e^{v_{BC}/V_T} - 1) \quad (14)$$

$$i_C = I_S (e^{v_{BE}/V_T} - 1) - \frac{I_S}{\alpha_R} (e^{v_{BC}/V_T} - 1) \quad (15)$$

$$i_B = \frac{I_S}{\beta_F} (e^{v_{BE}/V_T} - 1) + \frac{I_S}{\beta_R} (e^{v_{BC}/V_T} - 1) \quad (16)$$

where  $\beta_F$  ( $\beta_R$ ) is the forward (reverse) common-emitter current gain,

$$\beta_F = \frac{\alpha_F}{1 - \alpha_F}$$

$$\beta_R = \frac{\alpha_R}{1 - \alpha_R},$$

or equivalently

$$\alpha_F = \frac{\beta_F}{1 + \beta_F}$$

$$\alpha_R = \frac{\beta_R}{1 + \beta_R}. \quad (17)$$

In the normal mode of operation, ‘forward active’, the base-collector junction is reverse biased and  $v_{BC}$  is negative, so we can neglect the  $e^{v_{BC}/V_T}$  terms in (14–16); additionally

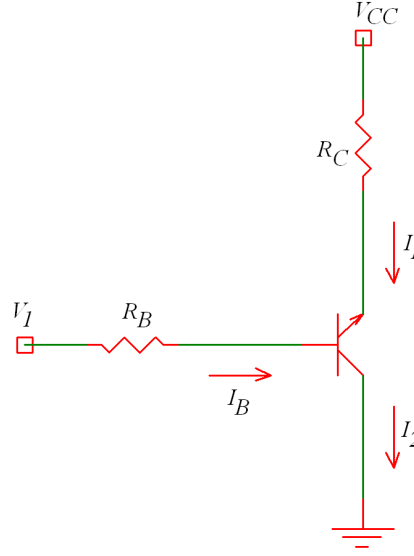


Figure 7: Reverse mode transistor operation.

the saturation current  $I_S$  is very small, so neglect solitary  $I_S$  terms and those with just  $I_S$  and a current gain; then dividing (15) by (16) gives the familiar expression

$$i_C = \beta_F i_B.$$

Saturation occurs when  $i_B$  is so big that the collector current,  $i_C$ , ‘can’t keep up’, so  $i_C < \beta_F i_B$ . In saturation, whether forward or reverse mode, both p-n junctions are forward biased: neglecting  $I_S$  terms as before, and substituting for  $\alpha_R$  from (17), (15) and (16) can be approximated as

$$i_C = I_S e^{v_{BE}/V_T} - I_S \left( \frac{1 + \beta_R}{\beta_R} \right) e^{v_{BC}/V_T} \quad (18)$$

$$i_B = \frac{I_S}{\beta_F} e^{v_{BE}/V_T} + \frac{I_S}{\beta_R} e^{v_{BC}/V_T}. \quad (19)$$

These expressions can be manipulated in order to find the saturation voltage,  $V_{CEsat}$ , as the difference between  $v_{BC}$  and  $v_{BE}$ , for either the forward or reverse saturation modes, and we now show the reverse case. Figure 7 shows a transistor operating in the reverse mode: the collector current is  $i_C = -I_2$ ; emitter current  $i_E = -I_1$ ; base current  $i_B = I_B$ ; and where  $I_2 = I_1 + I_B$ . Thus in the reverse active mode we would have  $I_1 = \beta_R I_B$ , and reverse saturation is when the base-emitter junction is forward biased, and  $I_1 < \beta_R I_B$ . Substitute for  $i_C$  in (18) and divide by (19) to get

$$\frac{-(I_1 + I_B)}{I_B} = \frac{e^{v_{BE}/V_T} - \left( \frac{1 + \beta_R}{\beta_R} \right) e^{v_{BC}/V_T}}{\frac{1}{\beta_F} e^{v_{BE}/V_T} + \frac{1}{\beta_R} e^{v_{BC}/V_T}}.$$

Factor out the  $e^{v_{BE}/V_T}$ :

$$\frac{-(I_1 + I_B)}{I_B} = \frac{1 - \left(\frac{1 + \beta_R}{\beta_R}\right) e^{(v_{BC} - v_{BE})/V_T}}{\frac{1}{\beta_F} + \frac{1}{\beta_R} e^{(v_{BC} - v_{BE})/V_T}},$$

cross-multiply,

$$\left(\frac{-I_1}{I_B} - 1\right) \left(\frac{1}{\beta_F} + \frac{1}{\beta_R} e^{(v_{BC} - v_{BE})/V_T}\right) = 1 - \left(\frac{1}{\beta_R} + 1\right) e^{(v_{BC} - v_{BE})/V_T},$$

gather terms,

$$e^{(v_{BC} - v_{BE})/V_T} \left(1 - \frac{I_1}{I_B \beta_R}\right) = \left(1 + \frac{1}{\beta_F} + \frac{I_1}{I_B \beta_F}\right),$$

and finally re-arrange and take logs to get

$$v_{BC} - v_{BE} = V_{ECsat} = V_T \log \frac{1 + \frac{1}{\beta_F} + \frac{I_1}{I_B \beta_F}}{1 - \frac{I_1}{I_B \beta_R}}. \quad (20)$$

This is equation (4.115) in section 4.13 of [5]—what would be really useful for our present purposes is some measure of the equivalent resistance,  $V_{ECsat}/I_1$ , as a function of the base current,  $I_B$ .

Starting with the numerator of the log term on the right-hand side of equation (20), for a transistor with a decent forward current gain, we'll have  $\beta_F \gg \beta_R > 1$ , and in reverse saturation,  $I_1 < \beta_R I_B$  or  $I_1/I_B < \beta_R$ , so we have

$$\frac{1}{\beta_F} \ll 1 \quad \text{and also} \quad \frac{I_1}{I_B \beta_F} < \frac{\beta_R}{\beta_F} \ll 1,$$

so ignore these terms to get

$$V_{ECsat} \approx V_T \log \frac{1}{1 - \frac{I_1}{I_B \beta_R}}.$$

In the denominator we also have

$$\frac{I_1}{I_B \beta_R} < 1$$

by the saturation condition, so now using the standard expansion

$$\frac{1}{1+x} = 1 - x + x^2 - x^3 + x^4 - \dots \quad -1 < x < 1,$$

further approximate to

$$V_{ECsat} \approx V_T \log \left(1 + \frac{I_1}{I_B \beta_R}\right).$$

Finally, using another standard expansion

$$\log(1+x) = x - \frac{x^2}{2} + \frac{x^3}{3} - \frac{x^4}{4} + \dots \quad -1 < x \leq 1,$$

we get

$$V_{ECsat} \approx V_T \frac{I_1}{I_B \beta_R},$$

to give

$$\frac{V_{ECsat}}{I_1} \approx \frac{V_T}{I_B \beta_R}, \quad (21)$$

which is an expression of the form that we were seeking—the collector-emitter resistance as a function of the base current.

After all these approximations, it is natural to ask whether the above expression bears any resemblance to reality. To answer that properly would require a ‘parametric analyzer’, to characterize the given transistor in its reverse region of operation. Needless to say one of these isn’t among my few pieces of lab equipment, but the answer can be glimpsed through SPICE simulation, and comparison of calculated values versus measurements from real hardware. The latter will have to wait for the second phase of this investigation, but I have done the former using SIMetrix.

The SPICE BJT model is very similar to that we started from above (taken from [5]), so as long as the reverse parameters are specified for the transistor of interest, we may get something of use. The parameters are  $BR$ ,  $NR$ ,  $ISC$ ,  $IKR$ ,  $NC$  and  $VAR$ —see for example [1] or [7]—and  $BR$ , the reverse current gain, corresponds to  $\beta_R$  used in the calculations above. In the Korg35 chip, the transistors of concern are 2SC1623 types, and fortunately the PSpice model of this transistor does have the reverse parameters defined: in particular  $BF = 206.7 \equiv \beta_F$  and  $BR = 4.210 \equiv \beta_R$ .

So the very simple circuit at the top of Figure 8 was entered into SIMetrix, driving the transistor with the collector and emitter swapped. A DC sweep of source  $V1$  was performed from 0 to 200mV, as the base current  $I1$  was stepped (logarithmically) from  $1\mu\text{A}$  to  $10\mu\text{A}$ : plots of the emitter voltage against the emitter current from the simulation run are shown in the middle set of traces. The traces show the classic BJT behaviour (albeit in the reverse region): nearer the origin the transistor is saturated, and as we move away and the lines become vertical, the transistor enters the active region. Mathematica was used to generate data from both the main reverse saturation expression and its approximation, equations (20) and (21) above, for one particular value of base current,  $I_B = 6.31\mu\text{A}$ , using  $V_T = 25\text{mV}$  and with  $\beta_F$  and  $\beta_R$  from the SPICE model as above. The data was then imported into SIMetrix and plotted alongside the equivalent simulation curve, the bottom set of traces in the figure. It can

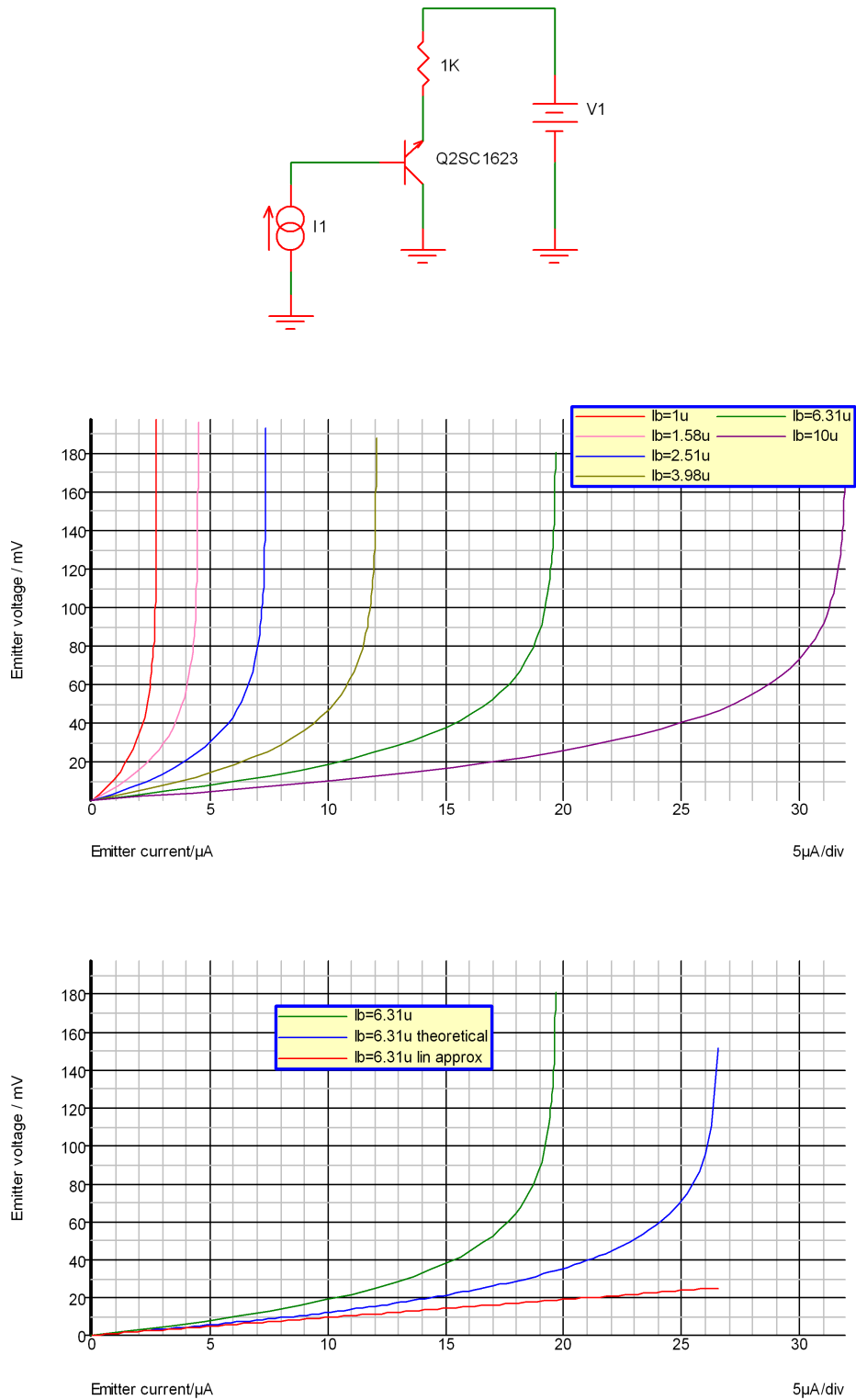


Figure 8: Comparison of BJT reverse saturation characteristics: simulation circuit (top); simulation output (middle); comparison of simulated, analytic and approximated data (bottom).

be seen that the simulation and analytic data are not really in that good agreement, most probably due to the less sophisticated model used in the above analysis. However, the linear approximation to the initial slope of the curve, i.e. the resistance, is actually quite passable, and is certainly more than capable of providing some assistance to both understanding the filter operation, and as an aid to predicting filter performance, which follows at the end of Section 3.2 below.

### 3.2 Exponential control

In Section 2.1, during the derivation of the transfer function for the OTA version, we made the substitution  $\omega_c = Kk/C_1$  at equation (3), where  $K = 19.2I_{abc}$ , and  $k$  derives from the scaling of the resistors at the inputs of the OTA. Thus we have

$$\omega_c = 2\pi f_c = \frac{Kk}{C_1} = \frac{19.2I_{abc}k}{C_1},$$

from which we see that the filter cut-off frequency  $f_c$  is directly proportional to the applied current  $I_{abc}$  driving the OTA:

$$f_c \propto I_{abc} \quad \text{or} \quad f_c = k_\alpha I_{abc},$$

where the constant of proportionality  $k_\alpha = 19.2k/(2\pi C_1)$ . For the Korg35-based version, we have  $\omega_c = 1/RC$ , first introduced at equation (2), but used implicitly throughout the Sallen-Key/Korg35 transfer function derivation in Section 2.2. Then in Section 3.1 at equation (21) we (tentatively!) derived an approximation for the equivalent resistance of the transistors in the Korg35 chip:

$$R_{equiv} = \frac{V_{ECsat}}{I_1} \approx \frac{V_T}{I_B\beta_R}, \quad (22)$$

and these act as the resistances of the equivalent ‘RC’ stages, so in this case we have

$$\omega_c = 2\pi f_c = \frac{1}{RC} = \frac{I_B\beta_R}{V_TC}, \quad (23)$$

and once again we have that the cut-off frequency is directly proportional to an applied current (in this case  $I_B$ ):

$$f_c \propto I_B \quad \text{or} \quad f_c = k_\beta I_B,$$

where  $k_\beta = \beta_R/(2\pi V_TC)$ . Thus in either case we can control the cut-off frequency,  $f_c$ , by controlling a current.

It turns out that to help make a voltage-controlled filter musically useful, it is convenient to control the cut-off frequency,  $f_c$ , *exponentially* with respect to an input voltage,  $V_{in}$ , and often a ‘1V/octave’ control law is used, i.e.

$$f_c = f_0 2^{V_{in}},$$

where  $f_0$  is the cut-off frequency with no input,  $V_{in} = 0$ , and so we see that the cut-off frequency doubles, i.e. increases by an octave, for every 1V of input:

$$\begin{aligned} f_c &= f_0 2^0 = f_0 && \text{for } V_{in} = 0 \\ &= f_0 2^1 = 2f_0 && = 1 \\ &= f_0 2^2 = 4f_0 && = 2, \text{ etc.} \end{aligned}$$

By writing

$$f_c = f_0 2^{V_{in}} = f_0 (e^{\log 2})^{V_{in}} = f_0 e^{0.69V_{in}}$$

where  $e = 2.71828\dots$ , the base of natural logarithms, this exponential relationship becomes even clearer.

It is incredibly fortuitous then that the current through a standard  $p$ - $n$  semiconductor junction is exponentially related to the voltage across it: how this is achieved in the Korg35 chip is detailed next; the OTA version uses a standard type of exponential converter, which is briefly mentioned later. The exponential current output from either mechanism is then used to control the frequency, as outlined at the beginning of this section, thus providing the overall exponential control of the frequency that is desired.

The circuit at the top of Figure 9 shows the basic idea of how an exponential relationship is achieved in the Korg35 chip:  $D_1$  represents the base-collector junction of transistor  $Q_1$  in the Korg35, and similarly  $D_2$  for  $Q_2$ . By varying the voltage  $V_{in}$ , the total current  $I$  through the resistor is split symmetrically through the diodes, currents  $I_1$  and  $I_2$ : when  $V_{in}$  is sufficiently negative,  $D_2$  does not conduct, and all the current flows through  $D_1$ ; as  $V_{in}$  is increased,  $D_2$  starts to conduct and ‘robs’ some of the current from  $D_1$ ; when  $V_{in}$  is sufficiently large and positive,  $D_1$  stops conducting and all the current flows through  $D_2$ . The simulation traces in Figure 9 show the three currents as the voltage  $V_{in}$  is swept from  $-500\text{mV}$  to  $+500\text{mV}$ : clearly the relationship between the currents and  $V_{in}$  is similar to that for the standard differential pair, and is based on the hyperbolic tangent:

$$\begin{aligned} I_1 &= \frac{I}{2} \left[ 1 - \tanh \left( \frac{V_{in}}{2V_T} \right) \right], \\ I_2 &= \frac{I}{2} \left[ 1 + \tanh \left( \frac{V_{in}}{2V_T} \right) \right]. \end{aligned}$$

(The derivation of this is not worked here, as what follows below is very similar—the equivalent for the differential pair may be found in [6], which is based on a method found in [8].)

It can be seen that if  $V_{in}$  is restricted to be below about  $-50\text{mV}$ , then current  $I_2$  (blue in Figure 9) has the required (approximate) exponential relationship to  $V_{in}$ . This

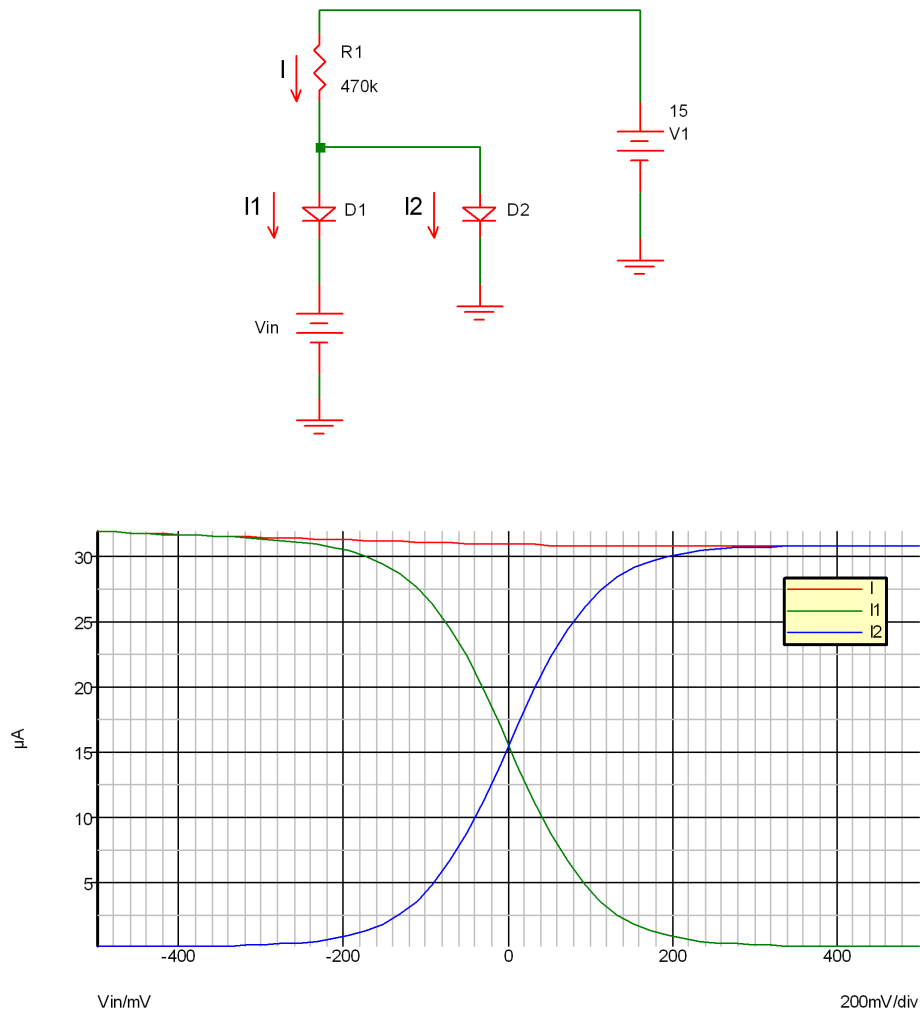


Figure 9: Achieving basic exponential control

can be shown more formally, as by definition

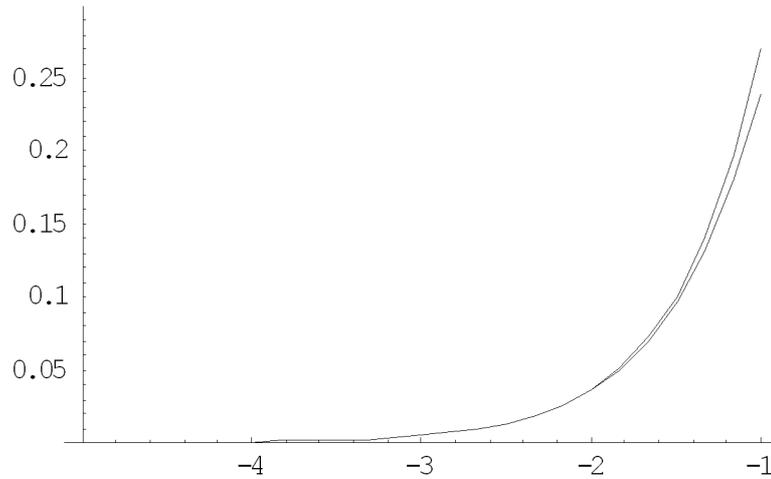
$$\tanh x = \frac{e^x - e^{-x}}{e^x + e^{-x}} = \frac{e^{2x} - 1}{e^{2x} + 1},$$

and using the approximation

$$(1 + x)^{-1} = 1 - x + x^2 - x^3 + x^4 - \dots, \quad |x| < 1,$$

then

$$\begin{aligned} (e^{2x} - 1)(e^{2x} + 1)^{-1} &\approx (e^{2x} - 1)(1 - e^{2x} + e^{4x} - \dots) \\ &= e^{2x} - e^{4x} - 1 + e^{2x} - e^{4x} + \dots \\ &= -1 + 2e^{2x} - 2e^{4x} \dots \end{aligned}$$

Figure 10: Approximation of  $2e^{2x}$  (upper curve) by  $1 + \tanh x$ 

as long as  $|e^{2x}| < 1$ , and if this is the case, then the higher-order terms in  $e$  are even smaller, so neglect them to give

$$\tanh x \approx -1 + 2e^{2x}$$

or more usefully

$$1 + \tanh x \approx 2e^{2x}. \quad (24)$$

The condition  $|e^{2x}| < 1$  just translates into  $x < 0$ , but the closeness of the approximation also depends on the omitted terms: a visual check of this is shown in Figure 10 which shows  $1 + \tanh x$  plotted with  $2e^{2x}$ , whereupon it seems clear that the approximation is going to be close enough for the purposes of controlling the cut-off frequency of the filter!

Thus current  $I_2$  gives the kind of exponential relationship we want

$$I_2 \approx \frac{I}{2} \left[ 2e^{2\left(\frac{V_{in}}{2V_T}\right)} \right] = Ie^{\left(\frac{V_{in}}{V_T}\right)}.$$

However this doesn't reflect the fact that the Korg35 chip has the three diodes/transistors in it's set-up, so a slightly more complicated model is needed—the workings of this model are almost identical to the preceding, and so are the outcomes, with one exception which may be the reason for the unequal capacitor values used in the filter, and so it will be expounded in full.

On the left in Figure 11 is a simplified representation of the relevant transistors in the Korg35, and on the right is the model we'll use to represent them. Voltage  $V_b$  is introduced to represent the extra voltage below  $D_3$  (not present for  $D_2/Q_2$ ) caused by the emitter-collector drop of  $Q_2$ , and which we will consider to be constant in the

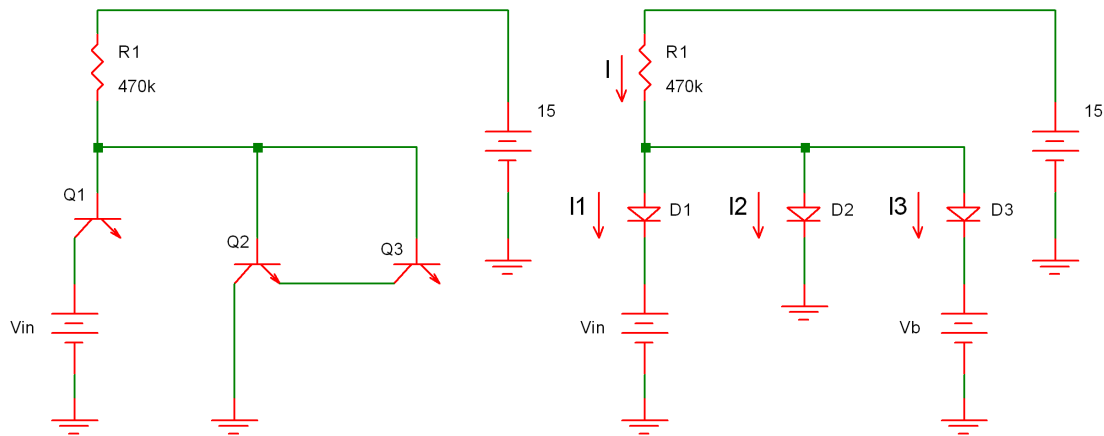


Figure 11: The three-transistor arrangement, and a model for it

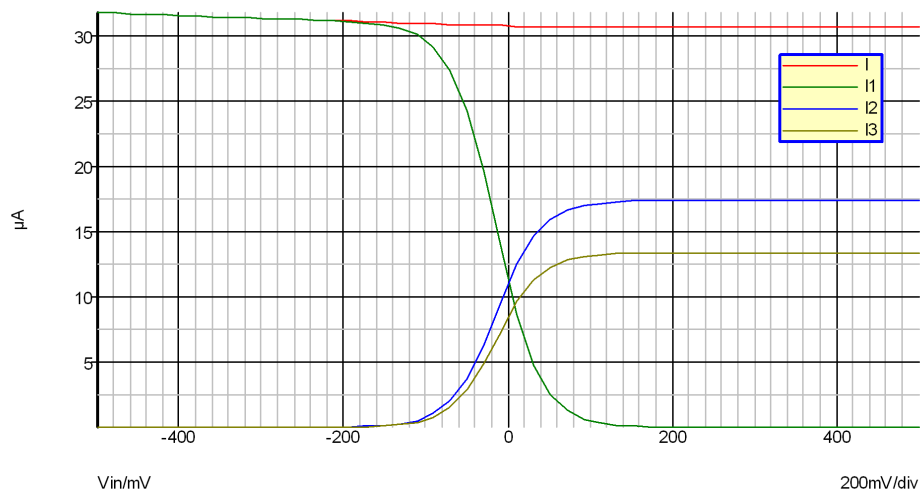


Figure 12: Currents in the three-transistor arrangement

following analysis. Figure 12 shows the four currents from a simulation run of the left (transistor) circuit in Figure 11: as one would expect in comparison with Figure 9, due to the third diode/transistor, the symmetry has been upset, and now (roughly) the sum of currents through  $D_2/Q_2$  and  $D_3/Q_3$  now balance that through  $D_1/Q_1$ ; note also that  $I_3$  is slightly less than  $I_2$ , which is due to the voltage  $V_b$  we have introduced in the diode model. We will now derive some expressions for these currents.

Annotate the voltage at the node joining the diodes to  $R_1$  as  $V_a$ . Assume the saturation currents of all three diodes to be  $I_s$ , and using the standard Ebers-Moll

model, we can formulate the currents as:

$$I = I_1 + I_2 + I_3 \quad (25)$$

$$I_1 = I_s e^{\frac{V_a - V_{in}}{V_T}} \quad (26)$$

$$I_2 = I_s e^{\frac{V_a}{V_T}} \quad (27)$$

$$I_3 = I_s e^{\frac{V_a - V_b}{V_T}} \quad (28)$$

For  $I_2$ : divide (26) by (27); (28) by (27); and substitute back into (25):

$$\begin{aligned} \frac{I_1}{I_2} &= e^{-\frac{V_{in}}{V_T}}, & \text{so } I_1 &= I_2 e^{-\frac{V_{in}}{V_T}} \\ \frac{I_3}{I_2} &= e^{-\frac{V_b}{V_T}}, & \text{so } I_3 &= I_2 e^{-\frac{V_b}{V_T}} \end{aligned}$$

then

$$I = I_2 e^{-\frac{V_{in}}{V_T}} + I_2 + I_2 e^{-\frac{V_b}{V_T}},$$

so

$$I_2 = \frac{I}{1 + e^{-\frac{V_b}{V_T}} + e^{-\frac{V_{in}}{V_T}}} = \frac{I}{A + e^{-\frac{V_{in}}{V_T}}}$$

where we have substituted

$$A = 1 + e^{-\frac{V_b}{V_T}}$$

for notational simplicity. Factor the  $A$  out:

$$I_2 = \frac{I}{A \left( 1 + \frac{e^{-\frac{V_{in}}{V_T}}}{A} \right)} = \frac{I}{A \left( 1 + e^{-\frac{V_{in}}{V_T} - \log A} \right)}, \quad (29)$$

multiply top and bottom by 2, and add zero into the top

$$I_2 = \frac{I \left( 1 + 1 + e^{-\frac{V_{in}}{V_T} - \log A} - e^{-\frac{V_{in}}{V_T} - \log A} \right)}{2A \left( 1 + e^{-\frac{V_{in}}{V_T} - \log A} \right)},$$

then divide

$$\begin{aligned} I_2 &= \frac{I}{2A} \left( 1 + \frac{1 - e^{-\frac{V_{in}}{V_T} - \log A}}{1 + e^{-\frac{V_{in}}{V_T} - \log A}} \right) \\ &= \frac{I}{2A} \left( 1 + \tanh \frac{1}{2} \left( \frac{V_{in}}{V_T} + \log A \right) \right). \end{aligned} \quad (30)$$

The working for  $I_3$  is similar: dividing (26) by (28), (27) by (28) and substituting into (25) gives

$$I = I_3 e^{\frac{-V_{in} + V_b}{V_T}} + I_3 e^{\frac{V_b}{V_T}} + I_3,$$

which re-arranges to

$$I_3 = \frac{I}{B \left( 1 + e^{\frac{-V_{in} + V_b}{V_T}} \right)}$$

where

$$B = 1 + e^{\frac{V_b}{V_T}}.$$

In comparison with (29) and (30) above, this can be seen to be

$$I_3 = \frac{I}{2B} \left( 1 + \tanh \frac{1}{2} \left( \frac{V_{in} - V_b}{V_T} + \log B \right) \right). \quad (31)$$

It is the ‘ $-V_b$ ’ term inside the tanh in this last expression which causes the  $I_3$  curve to lie a little below  $I_2$  in Figure 12—this is made more obvious below when the approximation to the exponential is made, but note that from both the expressions for  $I_2$  and  $I_3$  the apparent ‘halving’ of  $I_1$  is not seen, so first we work  $I_1$ , just as a ‘sensitivity’ check. In order to simplify the working, assume that  $V_b = 0$ : this in turn means that both  $A = B = 2$ . Then similar to before, divide (27) by (26); (28) by (26); and substitute back into (25), so that

$$I = I_1 + I_1 e^{\frac{V_{in}}{V_T}} + I_1 e^{\frac{V_{in}}{V_T}},$$

and

$$I_1 = \frac{I}{1 + 2e^{\frac{V_{in}}{V_T}}}$$

to give (again by comparison with (29) and (30) worked above for  $I_2$ )

$$I_1 = \frac{I}{2} \left( 1 - \tanh \frac{1}{2} \left( \frac{V_{in}}{V_T} + \log 2 \right) \right)$$

and the other two are now identical, since  $V_b = 0$  and  $A = B = 2$

$$I_2 = I_3 = \frac{I}{4} \left( 1 + \tanh \frac{1}{2} \left( \frac{V_{in}}{V_T} + \log 2 \right) \right),$$

from which the halving effect *is* now abundantly clear, due to the ‘ $I/4$ ’ factor, rather than the ‘ $I/2$ ’ of the  $I_1$  expression.

If we ensure that  $V_{in}$  is sufficiently negative, we can use the approximation (24) on the  $I_2$  and  $I_3$  expressions (30) and (31) to get

$$\begin{aligned} I_2 &\approx \frac{I}{A} \left( e^{\frac{V_{in}}{V_T} + \log A} \right) = I e^{\frac{V_{in}}{V_T}} \\ I_3 &\approx \frac{I}{B} \left( e^{\frac{V_{in} - V_b}{V_T} + \log B} \right) = I e^{\frac{V_{in} - V_b}{V_T}} = k I e^{\frac{V_{in}}{V_T}} \end{aligned} \quad (32)$$

where  $k = e^{-V_b/V_T}$ , and which will be less than one as long as  $V_b > 0$ , being in broad agreement with the simulation traces in Figure 12. This is what we want: at the start of

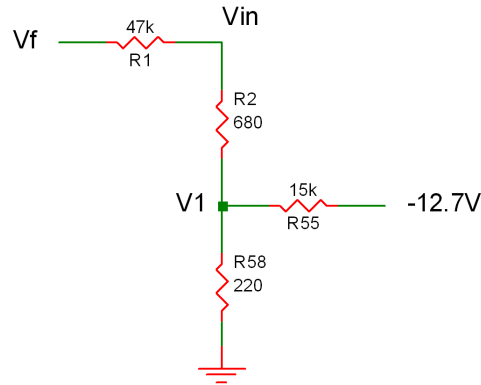


Figure 13: Input scaling of frequency control voltage (Korg35 version)

the section we saw that the cut-off frequency is directly related to the current through the transistors (via the ‘equivalent resistance’), and the current is exponentially related to an input voltage, thus giving exponential control of the frequency. What is more, from equation (22) at the beginning of the section, the equivalent resistance of the transistor is inversely proportional to the base current,  $I_B$  (given here by  $I_2$  and  $I_3$ ). Then since  $I_3 < I_2$ , the equivalent resistance of  $Q_3$  is greater than that of  $Q_2$ . Thus if we want to keep the cut-off frequencies of both the stages roughly the same, we will need to adjust the capacitors: (notating them as Figure 3) we thus require  $C_2 < C_1$ , which of course is exactly the situation in the actual circuit. This may be part of the reason why the capacitors are unequal: it is doubtful whether in reality the ‘ $k$ ’ in the above  $I_3$  expression is as much as the  $1/3$  factor seen for the capacitors in the real circuit, but then it is highly improbable that Korg did anywhere near this sort of analysis during the design of the filter, they would surely have been driven by empirical data, i.e. altered the  $C$  values until it sounded right, or maybe the 3-to-1 ratio was seen to give a better cut-off slope when plotted? (It is even tricky to make a comparison using simulation: making the capacitors equal shifts all the responses up in frequency, and also dramatically lowers the resonance for any given setting of the pot, due to the change of the ‘ $2\frac{1}{3}$ ’ constant to ‘3’, in the denominator of the transfer function.)

For the above exponential approximation to work, we saw that  $V_{in}$  needs to be small and negative—for practical use then, we need to suitably scale the input control voltage before inputting it to the Korg35 chip. Figure 13 shows the network which achieves this. Let the input frequency control voltage be  $V_f$ : we thus require  $V_{in}$  in terms of this; the -12.7V voltage is derived from a ‘DC operating point’ SPICE simulation. Nodal analysis at the  $V_{in}$  node:

$$\frac{V_f}{47} + \frac{V_1}{0.68} = V_{in} \left( \frac{1}{47} + \frac{1}{0.68} \right).$$

Ignore the  $1/47$  on right as it is much smaller than the other term, then multiply

throughout by 47:

$$V_f + 69V_1 = 69V_{in}.$$

At the  $V_1$  node:

$$\frac{V_{in}}{0.68} - \frac{12.7}{15} = V_1 \left( \frac{1}{0.68} + \frac{1}{15} + \frac{1}{0.22} \right)$$

Again, ignore the  $1/15$  term on the right, then multiply throughout by 15:

$$22V_{in} - 12.7 = 90V_1,$$

and then eliminate  $V_1$  between the two expressions

$$V_f + \frac{69}{90}(22V_{in} - 12.7) = 69V_{in}.$$

Re-arranging then gives

$$V_{in} = \frac{V_f}{52} - 0.2.$$

This gives  $V_{in} \approx -300\text{mV}$  for  $V_f = -5\text{V}$ , and  $V_{in} \approx -100\text{mV}$  for  $V_f = +5\text{V}$ , i.e.  $V_{in}$  is small and negative as required. If we substitute for  $V_{in}$  in (32) then we get

$$\begin{aligned} I_2 &= Ie^{\frac{V_{in}}{V_T}} = Ie^{-\frac{0.2}{V_T}} e^{\frac{V_f}{52V_T}} = I'e^{0.77V_f} \\ &\approx I'2^{V_f}, \end{aligned} \quad (33)$$

where  $V_T = 0.025$ , and we have rolled the constant involving it into  $I'$  (more exactly  $e^{0.77} = 2.12$ ). Thus  $V_f$  has a 1V/octave response with respect to the cut-off frequency.

Figure 14 shows the frequency responses from an AC simulation of the circuit in Figure 1, for  $V_4(\equiv V_f)$  in 1V steps from  $-5\text{V}$  to  $+5\text{V}$ : the 12dB/octave cut-off slope is clearly to be seen, and if we take the first 8 steps from  $\approx 22\text{Hz}$  to  $4900\text{Hz}$  (the last few clearly ‘bunch up’), we get

$$\log_2 \frac{4900}{22} = \frac{\log 4900/22}{\log 2} = 7.8 \text{ octaves},$$

thus demonstrating the 1V/octave relationship. (I suspect other circuitry within the MS10/MS20 may re-scale this, but I’ve not been that bothered to check in any detail.)

Finally to end this section, let’s put all the equations together to see how well they might predict the filter’s performance: put  $I_2$  from equation (33) as  $I_B$  in (23) to get

$$f_c = \frac{Ie^{-\frac{0.2}{V_T}} e^{\frac{V_f}{52V_T}} \beta_R}{2\pi V_T C},$$

where:  $I$  is the ‘reference current’ for the exponential converter through  $R_3$  (Figure 1), which we can approximate as  $15/470\text{k} = 32\mu\text{A}$ ; we take  $V_T = 0.025\text{mV}$ ; from the

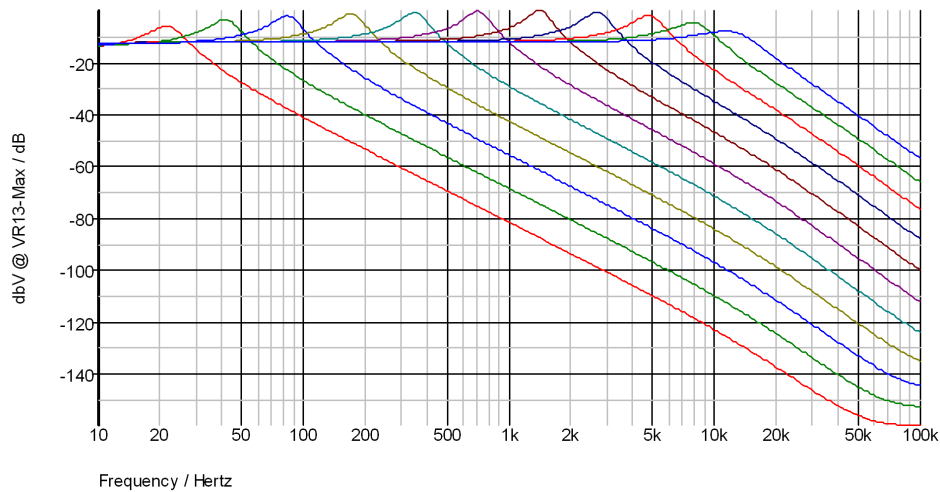


Figure 14: Frequency response of Korg35-based filter

SPICE model for the 2SC1623,  $\beta = 4.21$ ; and  $C = 3.3\text{nF}$ . Substituting these and calculating we get

$$f_c = 87.0 e^{V_f/1.3},$$

which for  $V_f = -5$  gives  $f_c = 2\text{Hz}$ , and  $V_f = +5$  gives  $f_c = 4070\text{Hz}$ , compared to approximately 22Hz and 12kHz for the simulation, from Figure 14. I actually think this is pretty good, considering all the approximations we have made down the line, from that for the equivalent resistance of the transistors, to approximating the exponentials in the exponential converter and so on. Certainly it should get you in the right ball-park for an initial choice of the capacitor values!

## 4 Asymmetrical Frequency and Resonance Responses of the Korg35

A simple transient analysis run of the circuit in Figure 1 shows another facet of the Korg35-based filter which isn't present in the later OTA version: the resonance is asymmetrical, being stronger for the negative half of the signal than for the positive half, as shown in the top trace of Figure 15. (For comparison a similar signal with similar settings from the OTA version is also given, and which shows the normal symmetrical shape.) This is caused by the signal itself interacting with the currents in the Korg35, affecting both the cut-off frequency and the resonance. From Section 3.2, we have that increasing the signal itself will reduce the current through the two transistors of the Korg35, effectively increasing their equivalent resistance, and in turn decreasing the frequency of the poles formed with their respective capacitors. This is barely

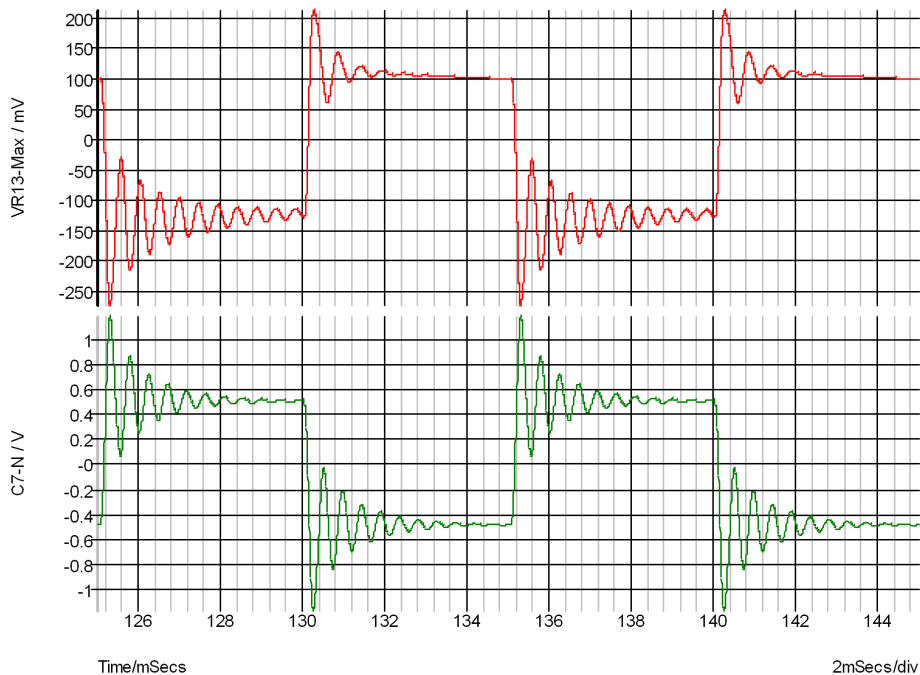


Figure 15: Uneven resonance response of Korg35 filter (top); similar signal for OTA version (bottom)

discernable in Figure 15, but measurements taken directly from the simulation show that the ‘positive’ ringing frequency is about 1.7kHz, whilst that for the negative half is around 2kHz. Whilst deriving the transfer function for the Korg35 filter, equation (8) in Section 2.2, we have already seen how changing the relative values of the  $R$ ’s and  $C$ ’s can have an effect on the constant on the  $s$ -term in the denominator (which ‘defines’ the resonance), so it is perhaps not so surprising that the magnitude and sign of the signal is also affecting the resonance in this way!

## 5 Non-Linear Effects of the Feedback Diodes

In both filter versions there are gain elements having back-to-back diodes in the (local) feedback loop, which introduce non-linearities into the gain structures of the filters. The effect of these diodes is to deliberately distort the signal being filtered, thus adding to the overall aural characteristics of the filter. There are considerable differences between the way these are implemented in both filters: in the Korg35 version there are single back-to-back diodes in the main gain element of the forward path; in the OTA version there are strings of three diodes back-to-back in the gain element in the feedback path. In this section we’ll examine the effects of these diodes, starting with their general effect on the non-inverting op amp set-up in which they appear in both filters.

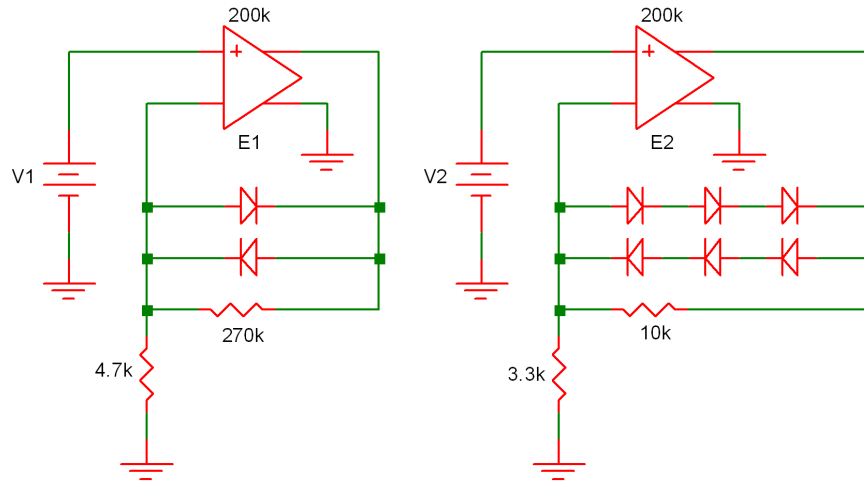


Figure 16: Gain-limiting diodes: Korg35 version (left); OTA version (right)

Figure 16 shows idealized representations of the circuit elements containing the diodes:  $E_1$  and  $E_2$  are high-gain voltage-controlled voltage-sources representing the appropriate op amps; capacitors maintaining DC levels have been omitted. In such an arrangement, if the input voltage is sufficiently small such that the diodes don't conduct (i.e. the input is approximately the total diode drop divided by the gain of the op amp set-up), this operates as a normal non-inverting op amp with its gain as appropriate; once the output voltage is such that the diodes conduct, it basically works as a (unity-gain) voltage follower, albeit with a DC-offset given by the diode drop. Thus small input voltages are amplified by the nominal gain of the section; as the input increases, the gain falls away, until at larger voltages it is just unity. Both transfer functions of the above circuits show this behaviour, but with very different scales, as seen in Figure 17. For the Korg35 version the central section has a gain of  $(1 + 270/4.7) \approx 58$ ; also shown is the unity-gain line, to which the main line is parallel once the diodes are conducting, but a diode-drop (about 0.5V) away from it (1N4148 diodes were used in the simulations throughout this section). The OTA version has a central gain section of only  $1 + 10/3.3 = 4$ , and due to the string of three diodes in series, when they are conducting the combined drop is about 2V, giving a much less pronounced 'kink' in the curve. It seems quite tricky to make a meaningful comparison between the two, due to the large differences in gain and the single vs. three diodes matter, but Figure 18 shows how these circuits distort: in both cases the magnitude of the input signal was chosen to give roughly the diode drops at the output if the diodes weren't there, i.e.  $0.5/58 \approx 8\text{mV}$  for the Korg35 version, and  $2.1/4 \approx 525\text{mV}$  for the OTA version. The traces show the output with and without the diodes, along with the distortion measurement made by SIMetrix: the gain drops off as the magnitude increases, causing the output wave to be more 'rounded' at its extremities.

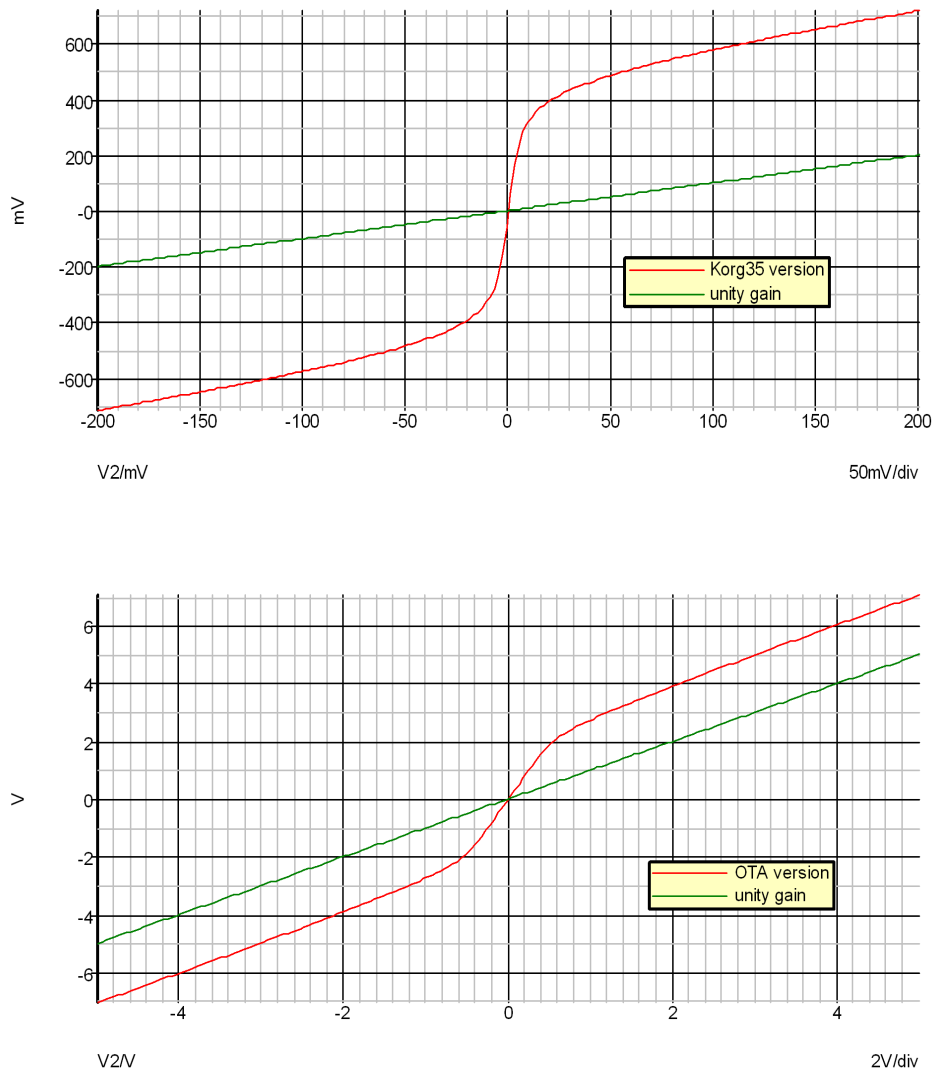


Figure 17: Diode limiter transfer functions: Korg35 (top); OTA (bottom)

As already noted, a major difference between the filters is where the diodes are located within the filter structure: in the Korg35 version they are in the forward path; in the OTA version they are in the feedback path. It seems highly likely that this will cause a significant difference in the filters' sound. To get some handle on what this difference might be, I did the following: AC analysis runs in SPICE are performed by finding the DC bias point, then non-linear elements like transistors, diodes etc. are linearized about this point (i.e. they are replaced with their small-signal models), and then the frequency sweep is performed. Thus any non-linear effects like clipping, distortion, saturation etc. will not be seen ([2]). To get around this I decided to see if I could deliberately introduce a DC signal that *would* bias the circuits into the non-linear regions of interest—Figure 19 gives the circuits I came up with. Both are again

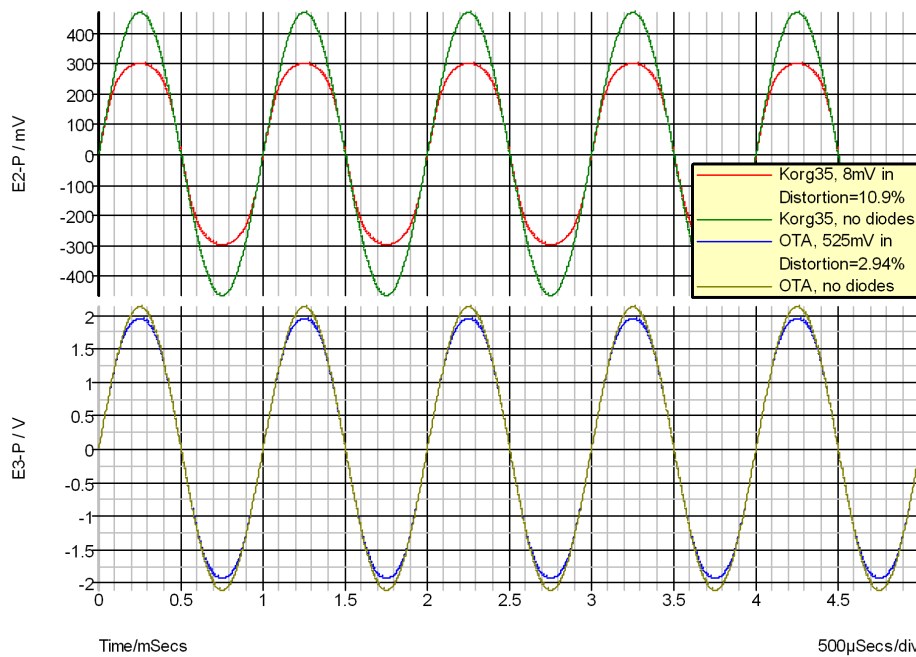


Figure 18: Diode limiter distortion: Korg35 (top); OTA (bottom)

idealized versions of the respective filter, and in both cases I have introduced voltage  $V_2$  at the input of the op amp which has the diodes: by performing AC sweeps whilst stepping  $V_2$ , I was able to get some idea of what would happen within each filter. The results of these sweeps are shown in Figure 20, and it is immediately obvious that they are quite different. I have interpreted these by thinking about what happens at *one* particular frequency whilst  $V_2$  is increased, i.e. equivalent to the signal magnitude being increased. For the Korg35 version it is clear that, no matter where we are in the spectrum (be it in the passband, around the cut-off frequency or in the reject band), then as the signal magnitude is increased the gain drops (as the diodes conduct more), and so that frequency will suffer progressive distortion. This seems to make sense to me: as the diodes are in the forward path, then signals of all frequencies will pass through them.

The picture for the OTA version is quite different: the only region affected by the increasing DC offset is that around the cut-off frequency (the 'corner'). Again, to me this seems to make sense: as the diodes are in the feedback path, only frequencies which are 'selected' by the feedback network will be affected by them. This difference also suggests a possible means of aurally detecting whether any particular Korg has the earlier or later filter: set the cut-off frequency fairly high and input a sine wave of much lower frequency; adjust the magnitude of the input signal; if the sound becomes 'richer' as the magnitude is increased (i.e. distortion is adding harmonics), then it could be

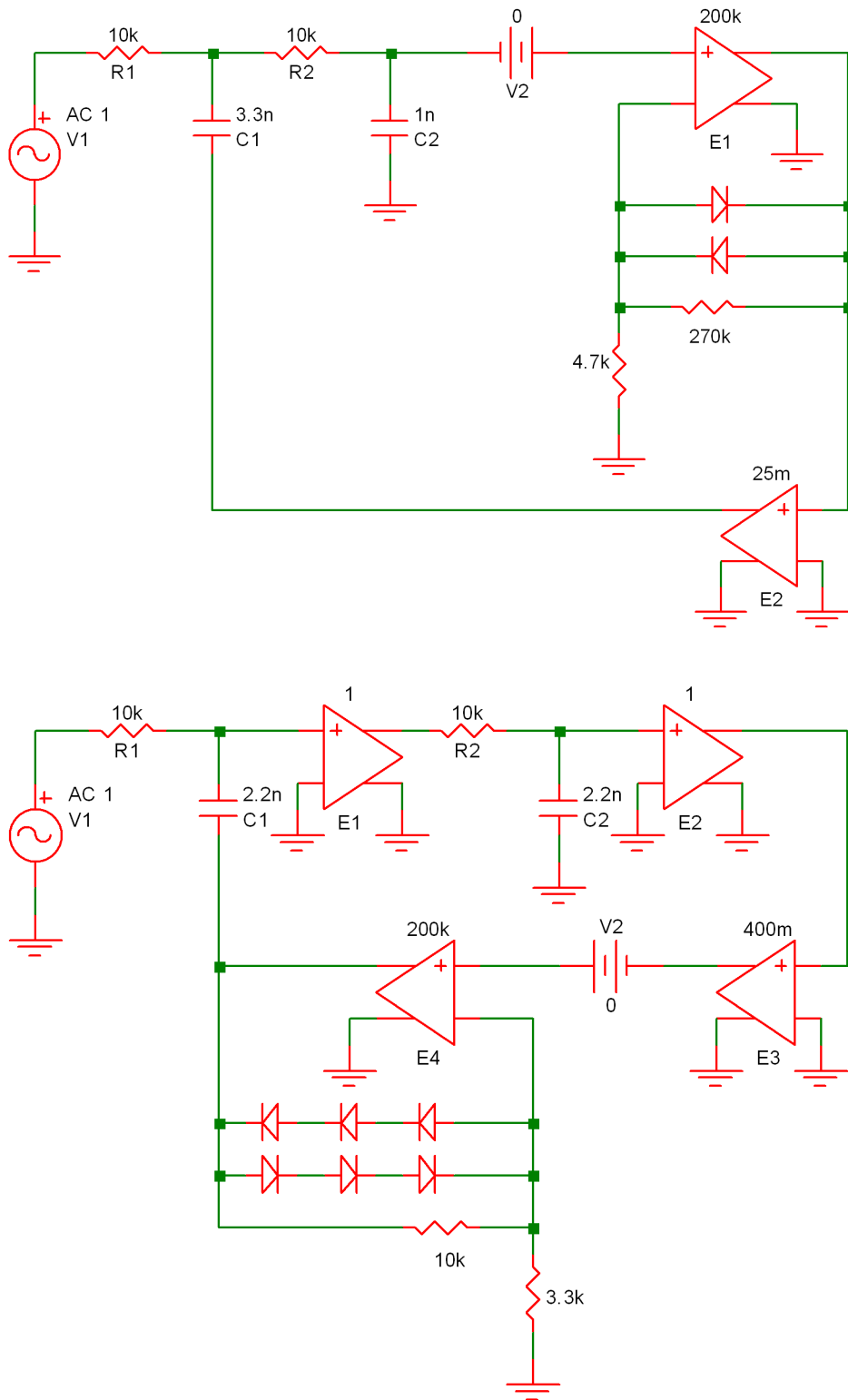


Figure 19: Circuits to help quantify the non-linear gains

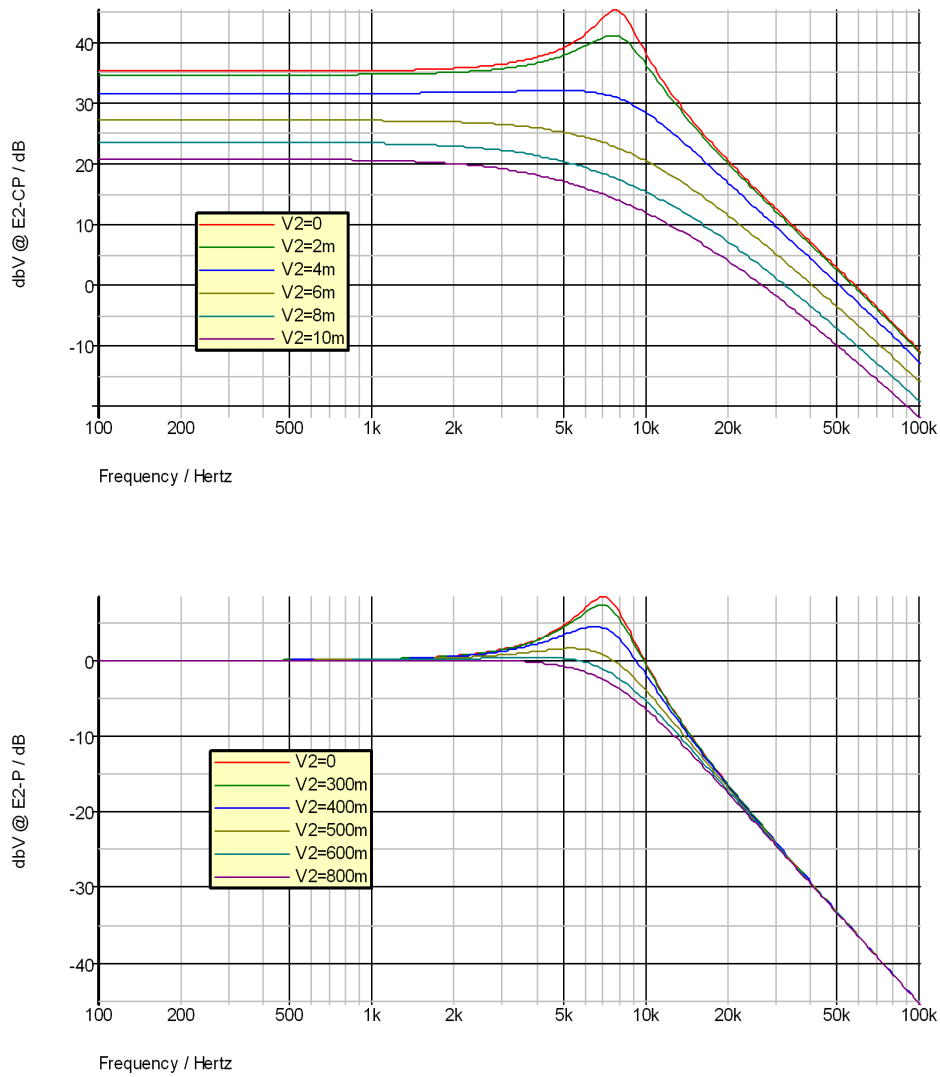


Figure 20: Gain reductions due to diode non-linearities

a Korg35 version; if the sound stays substantially the same, then chances are it is the later OTA version (and I must emphasize at this point that at the time of writing I have no way of checking this—there may be all manner of other distortions, e.g. in the OTA input stage, that might invalidate it!).

To double-check some of this thinking, I ran some transient analyses of the circuits in Figure 19 (with the AC source replaced with a sine wave). With the component values as shown, the cut-off frequencies were both around 7kHz, and there is a moderate amount of resonance in both cases (as suggested by the peaks in Figure 20). A 500Hz sine wave (i.e. well into the pass-band and away from the corner frequency), into the Korg35 version, with three different peak magnitudes, shows increasing amounts of

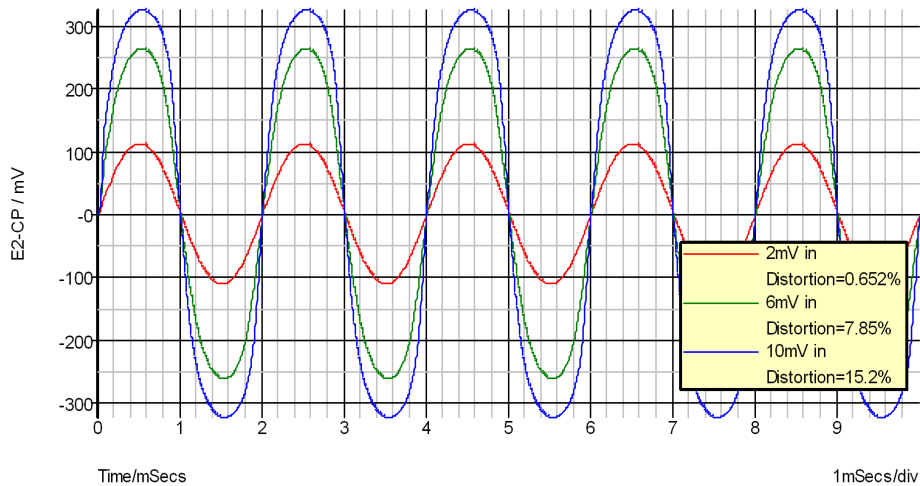


Figure 21: Korg35 transient analysis, 500Hz

distortion in Figure 21, which seems to corroborate Figure 20 nicely. Corresponding transient runs for the OTA version are shown in Figure 22, but the results are not as immediate. At the top is the output from a 500Hz sine wave, of three different magnitudes: even though this is well into the passband, there is still some residual distortion measured, due to the effect of resonance, which if lowered, makes the distortion go away. The middle set of traces shows a 5kHz wave: being much closer to the peak it does now exhibit distortion due to the diodes in the feedback loop. I was however a bit suspicious of the slight asymmetry of the distortion, and to ensure this wasn't due to some facet of the interaction of the fed back signal with the original one, I simply disconnected the diodes in the simulation, and the distortion basically disappears, as seen in the bottom set of traces. I'm reasonably convinced this reinforces how I'm thinking about the effects of the diodes, but the acid-test will be experimentation with some actual hardware!

## 6 Exponential Control in the OTA Version

Exponential control of the filter in the later OTA-based filters is by means of a standard exponential converter consisting of two PNP transistors and an op amp, the output of which drives the  $I_{abc}$  pins of the LM13600s. Having flogged through all the calculations, I was a little dismayed to discover that they produce (at the top end) current figures which are out by about a factor of two against the simulation. An AC simulation of the circuit in Figure 2 produces the traces shown in Figure 23: this is 10 steps of 0.5V each, from  $-2.5V$  to  $2.5V$ , into the  $47k\Omega$  resistor at the 'EXT CUT OFF FREQ' input on the schematics, which gave a reasonable looking spread, and I adjusted the voltage

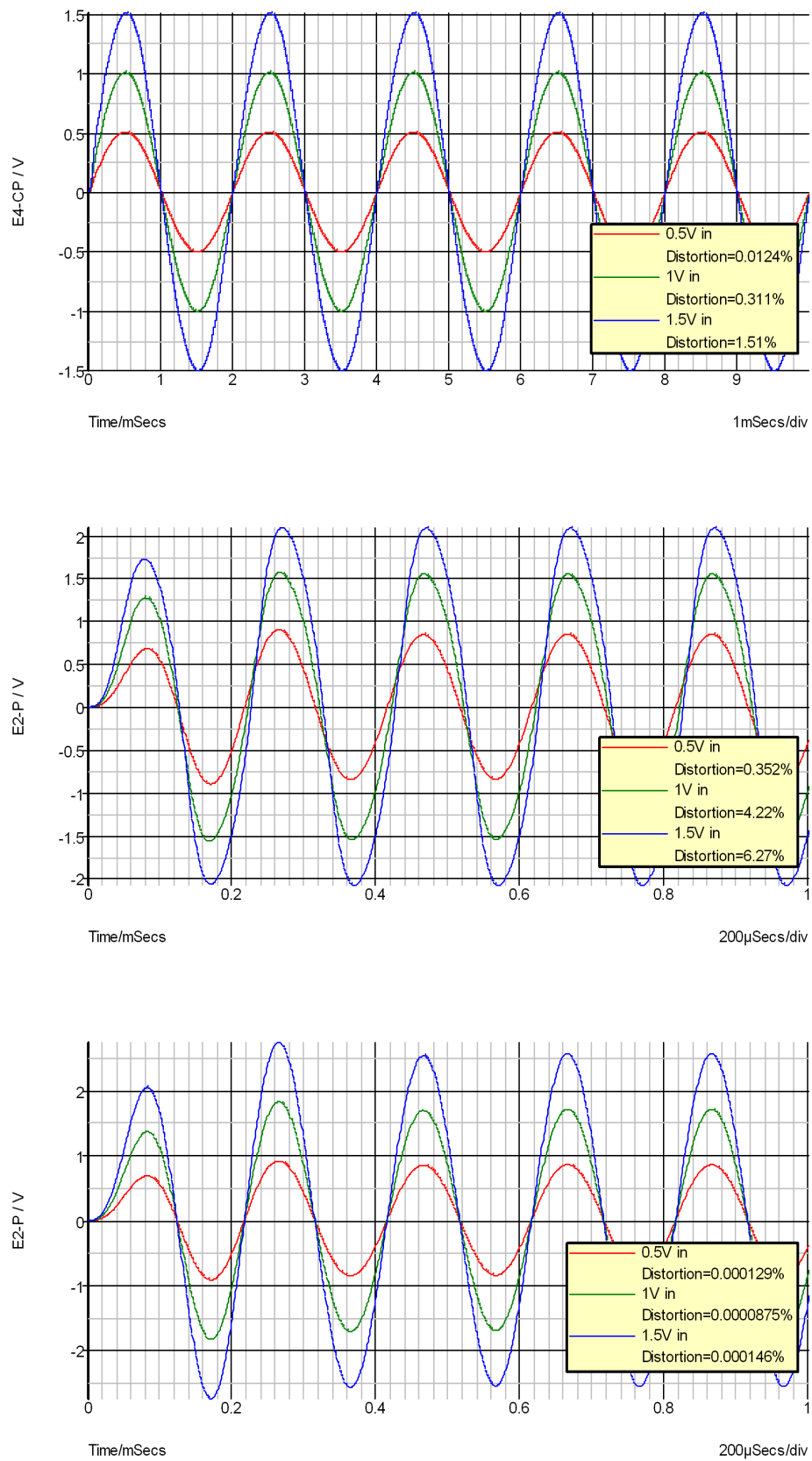


Figure 22: OTA transient analysis: 500Hz (top); 5kHz (middle); 5kHz, no diodes (bottom)

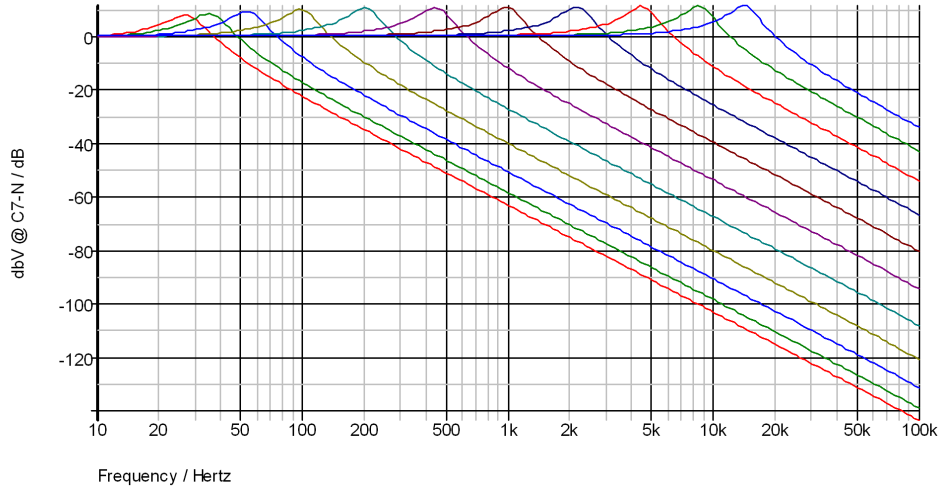


Figure 23: Frequency response of OTA-based filter

at the  $1\text{M}\Omega$  resistor accordingly to give a reasonable absolute alignment. The lower few steps are not evenly spaced, but if we take the 5 steps (i.e.  $2.5\text{V}$  in total) from  $100\text{Hz}$  to approximately  $4400\text{kHz}$ , this is

$$\log_2 \frac{4400}{100} = \frac{\log 4400/100}{\log 2} = 5.5 \text{ octaves,}$$

and so clearly 2 octaves/volt, or  $0.5\text{V}/\text{octave}$ , is intended! I was hoping that some calculations might bear this out, but the simulation gives about  $400\text{nA}$  to  $1\text{mA}$  output from the exponential converter, and the hand-calculations gave  $225\text{nA}$  to about  $2\text{mA}$ ! I suspect several reasons for this: at high currents, the ‘log conformity’ of the transistors will drop off (perhaps especially so since PNP?); I was ignoring any effects due to the base currents (which probably have some influence/are bigger than I was anticipating, again possibly exacerbated by the PNPs); I was taking no account of the dreaded ‘bulk emitter resistance’ which might also have been playing a role at such high currents.

In any case with so many control voltages being summed by such a simple passive network, and the fact that the  $2.2\text{k}\Omega$  resistor ( $R_{34}$ ) is *fixed*, and which would preferably be adjustable for some tweaking to the ‘control law’, this clearly isn’t going to be super-accurate! As a rough ‘guesstimate’, the input voltage is attenuated by (very roughly)  $2.2/47 = 1/21$ , and then comes through the converter as

$$e^{V_{in}/(21V_T)} = e^{1.9V_{in}} = 6.7^{V_{in}},$$

which is some way from the ‘4’ one would like to see for a 2 octave/volt law (but it is in the right direction). All-in-all I’m not bothered by this, as it plays such a little part in the main focus of the study.

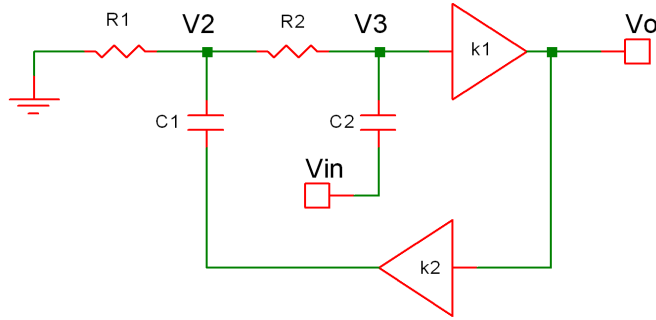


Figure 24: High-pass structure of the Korg35-based filter

## 7 The High-Pass Filter Variants are 6dB, not 12!

During development of the Doepfer A-106 MS20 filter clone, Dieter Doepfer noted that the high-pass configuration of the filter appeared to only have a 6dB/octave response, contrary to the normally reported figure of 12dB/octave. Simple calculation of the transfer function for the high-pass configuration shows that this assertion is indeed correct.

A device that can be employed to turn a low-pass filter into a high-pass one is to swap all frequency-determining  $R$ 's for  $C$ 's and  $C$ 's for  $R$ 's ([4]). Korg have not done this for either of the high-pass variants of the Korg35- and OTA-based filters in the MS20, but instead have grounded the normal (low-pass) input, and fed the input into the end of  $C_2$ , which has been lifted off ground—Figure 24 shows the resulting basic filter structure. The resulting high-pass filter does *not* have the 12dB/octave response that the  $RC$ - $CR$  transformation would give, but in fact only has a 6dB response, as we now show.

For simplicity set  $R_1 = R_2 = R$ , and  $C_1 = C_2 = C$ . As usual, nodal analysis at  $V_2$  gives

$$\frac{V_3}{R} + k_2 V_o s C = V_2 \left( \frac{1}{R} + \frac{1}{R} + s C \right),$$

which on putting  $\omega_c = 1/RC$  and using  $V_o = k_1 V_3$  becomes

$$V_o \left( \frac{1}{k_1} + k_2 \frac{s}{\omega_c} \right) = V_2 \left( 2 + \frac{s}{\omega_c} \right).$$

Nodal analysis at  $V_3$  gives

$$V_{in} s C + \frac{V_2}{R} = V_3 \left( \frac{1}{R} + s C \right),$$

and using the same substitutions,

$$V_{in} \frac{s}{\omega_c} + V_2 = \frac{V_o}{k_1} \left( 1 + \frac{s}{\omega_c} \right).$$

Now rid  $V_2$ :

$$V_o \left( \frac{1}{k_1} + k_2 \frac{s}{\omega_c} \right) = \left( \frac{V_o}{k_1} \left( 1 + \frac{s}{\omega_c} \right) - V_{in} \frac{s}{\omega_c} \right) \left( 2 + \frac{s}{\omega_c} \right).$$

Re-arranging gives

$$\begin{aligned} \frac{V_o}{V_{in}} &= \frac{k_1 \frac{2s}{\omega_c} + k_1 \frac{s^2}{\omega_c^2}}{\frac{s^2}{\omega_c^2} + (3 - k_1 k_2) \frac{s}{\omega_c} + 1} \\ &= \frac{2k_1 \frac{s}{\omega_c}}{\frac{s^2}{\omega_c^2} + (3 - k_1 k_2) \frac{s}{\omega_c} + 1} + \frac{k_1 \frac{s^2}{\omega_c^2}}{\frac{s^2}{\omega_c^2} + (3 - k_1 k_2) \frac{s}{\omega_c} + 1}. \end{aligned}$$

This transfer function represents a 6dB+6dB band-pass filter in parallel with a 12dB high-pass filter: above the cut-off frequency the band-pass will attempt to attenuate the signal at 6dB/octave, however the high-pass *will* pass the signal (effectively) unattenuated; below the cut-off the high-pass will attenuate at 12dB/octave, but the band-pass will only attenuate at 6dB/octave—the band-pass will ‘win’, and the signal is thus only attenuated by 6dB/octave. Thus the whole acts as a 6dB/octave high-pass filter. Note that I have rather ignored the effects of the ‘ $2k_1$ ’ and ‘ $k_1$ ’ gains in the numerators for this argument, but they really only affect the absolute gain levels, rather than the relative ones we are interested in—in any case, simple simulation confirms this situation. Figure 25 shows three SIMatrix ‘Laplace blocks’ containing the 3 transfer functions, band-pass, high-pass and combined, for  $k_1 = k_2 = 1$ , and the corresponding outputs. If the circuit of Figure 24 is also run with  $R_1 = R_2 = C_1 = C_2 = 1$  then its output response *exactly* over lies the blue ‘combined’ line of Figure 25.

## 8 Sallen-Key ‘Myths’ Discredited

**Myth 1.** Several times I’ve heard it expressed to the effect that ‘Sallen-Key filters are oscillators that also act as filters’. This is not entirely incorrect, for Sallen-Key filters have several impracticalities that normally mean they are not the best choice in filters. For a second order filter the reciprocal of the coefficient on  $s$  in the denominator is  $Q$ , the ‘quality factor’, which gives an indication of the amount of ‘peaking’ (i.e. resonance) at the cut-off frequency. For the Sallen-Key filter with equal  $R$ ’s and  $C$ ’s, we get from equation (7), with  $k_2 = 1$ ,

$$Q = \frac{1}{3 - k_1}.$$

This shows the first ‘problem’: we cannot choose  $Q$  independently from the amplifier gain,  $k_1$ , which is often inconvenient. Secondly, it is quite straightforward to show, [4],

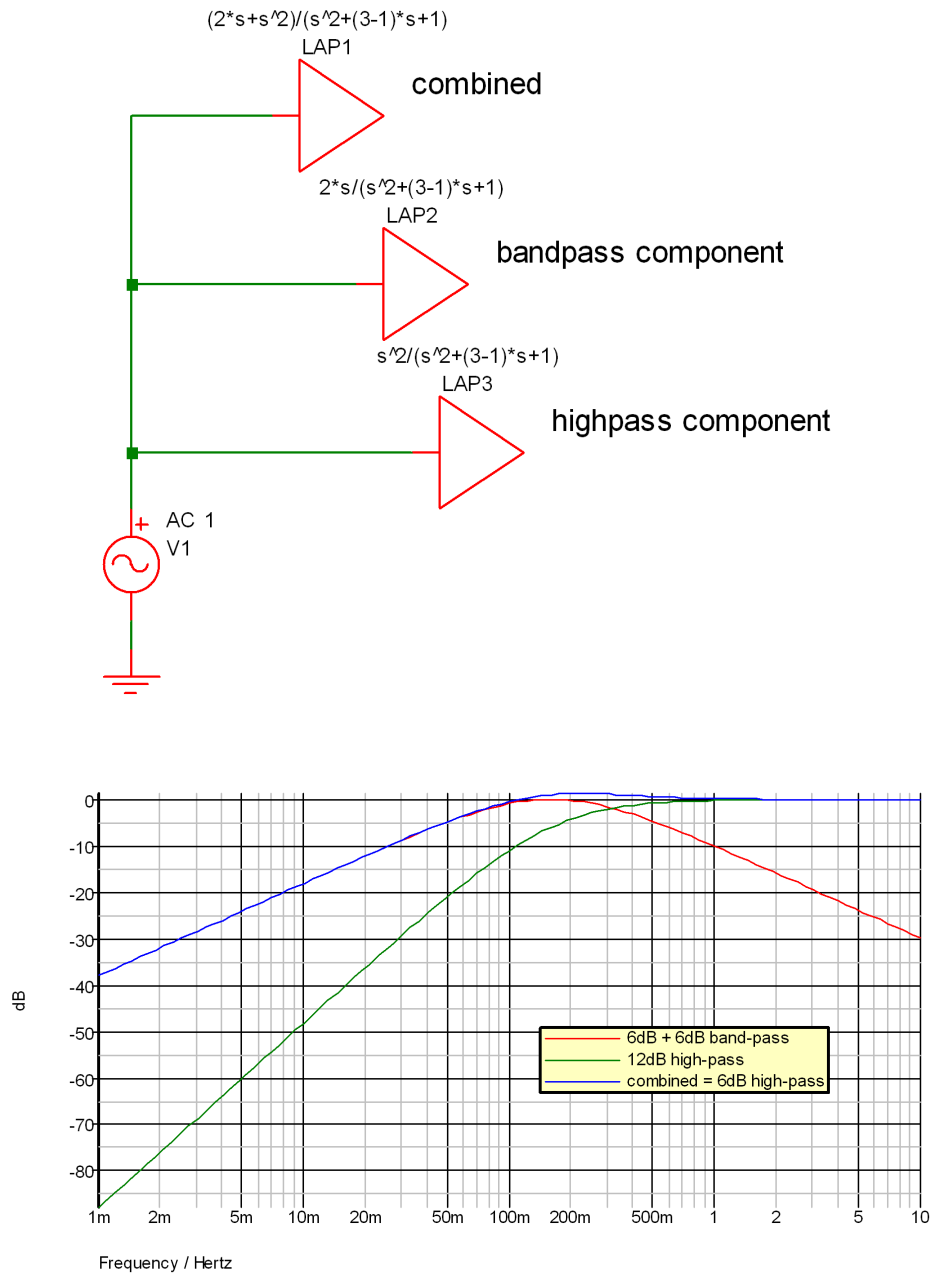
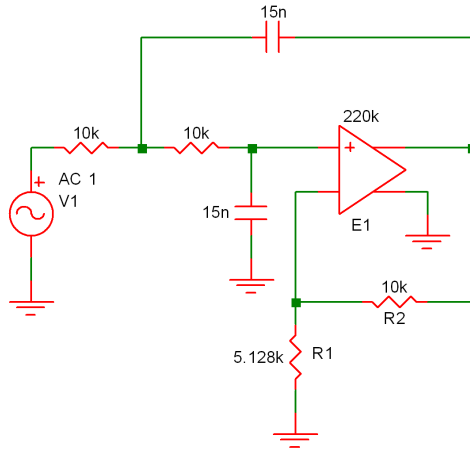


Figure 25: The individual high-pass components, and their responses

that  $Q$  is very sensitive to changes in the gain  $k_1$ :

$$\text{Percentage error in } Q = (3Q - 1) \times \text{percentage error in } k_1.$$

To illustrate this, suppose we want  $Q$  to be 20 in the following circuit:



Then the above says a 1% change in  $k_1$  produces  $\approx 60\%$  change in  $Q$ . Taking  $R_2$  as  $10\text{k}\Omega$ , then  $R_1$  is such that

$$20 = \frac{1}{3 - \left(1 + \frac{10\text{k}}{R_1}\right)},$$

which works out at  $R_1 = 5128\Omega$  (and which makes the gain  $k_1 \approx 3$ ). Then a 1% drop in  $R_1$  is  $5077\Omega$ , which gives

$$Q = \frac{1}{3 - \left(1 + \frac{10\text{k}}{5077}\right)} = 33,$$

and note this is not even a 1% change in  $k_1$ ! This is illustrated graphically in Figure 26 where I have plotted the magnitude response divided by 3 (the approximate gain,  $k_1$ , and note the linear scale) so that the peaks are roughly the  $Q$  values. Thus for the Sallen-Key filters, the sensitivity of  $Q$  to the components in the circuit is not very good, making it hard to reliably design a filter with high  $Q$ : if you try and do so, there is a good chance you'll get more  $Q$  than you bargained for, and the filter may well oscillate!

**Myth 2.** 'In Sallen-Key filters the resonance starts at the zero crossing.' This has nothing to do with the Sallen-Key structure *per se*, but is merely caused by the non-linear gain introduced by the back-to-back diodes. As illustrated by Figure 17 in Section 5, the gain of an op amp set-up with the diodes is greatest for small signals swinging around zero, with larger signals undergoing smaller changes in gain due to the effects of the diodes. Since the resonance depends on the gain, it is only natural

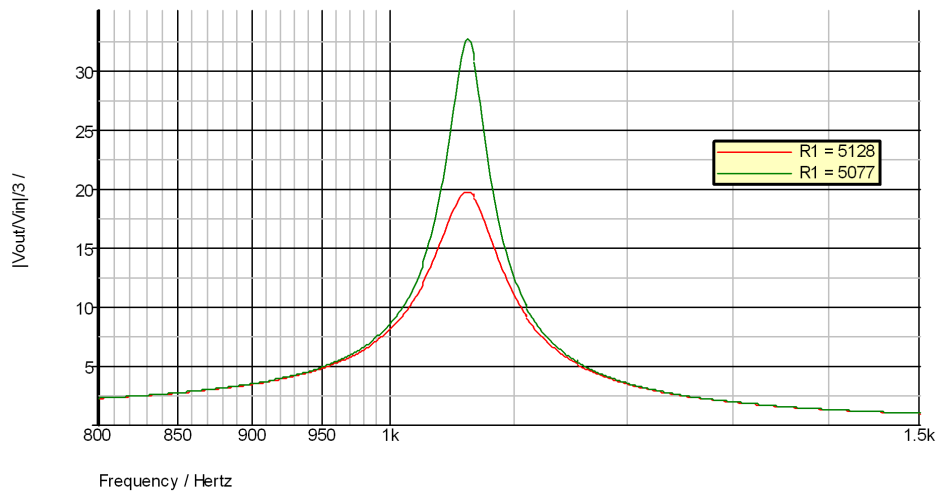


Figure 26: Change in  $Q$  (approximately the peak) for a 1% change in  $R_1$

that this should start to show itself near the zero crossing, as this *is* where the gain is highest. A simple (if somewhat contrived) example illustrates this: the circuit at the top of Figure 27 is the standard four-pole filter consisting of four buffered  $RC$  sections (such as the Moog ladder, CEM3320, SSM2040, and so on and so forth), which for oscillation requires a gain of 4 around the feedback loop. For the traces, input  $V_1$  is a 50Hz, 500mV peak-to-peak rising sawtooth (it is inverted by the input stage!);  $E_1$  and  $E_2$  are high-gain voltage-controlled voltage sources acting as op amps;  $E_1$  adds the input and the feedback;  $E_2$  and  $E_3$  combine to give the up-to-4 gain needed for high-resonance and oscillation (in order to get the diodes to work decently, the gain of  $E_2$  has been boosted, and is then brought back down to size by  $E_3$ ). So with the values shown, we see that the top trace in the figure exhibits the kind of behaviour we are talking about, and so this trait is not exclusively reserved for Sallen-Key filter topologies! If we remove the diodes and reduce the gain somewhat (to stop it oscillating completely!) by putting  $R_1 = 15k$ , then we ‘recover’ the usual behaviour of the filter ringing at the extremities of the signal swing.

## 9 Conclusion

We have seen that the two different filter versions do share some similarities, but there are also differences, perhaps the most notable being the position of the distortion-inducing diodes. But I feel that for now I have analysed the heck out of them, so I now intend to build three filters for side-by-side comparison: a clone of the Korg35 version; an OTA clone; and an OTA version with the proper Sallen-Key topology, but using back-to-back OTAs wired as voltage-controlled resistors (I have a rough and



ready simulation of this working, which suggests it is tractable). Hopefully when I have done this I shall be able to add further comments as to the efficacy of some of all this analysis!

One further question lingers though: what was it that made Korg ditch the Korg35 in favour of the OTA version? My two main guesses would be: the CV bleed-through on the Korg35 is probably pretty bad (simulation will probably show this, but I haven't tried it yet!); and for optimum performance the transistors in the chip would probably need to be matched, which must have added significantly to their manufacturing cost (or they simply made loads, and had a test to reject 'bad ones'—either way, it sounds costly).

## 10 Acknowledgements, Rights and Copyrights

The rights to the designs, and copyrights of the original schematics, obviously rest with Korg/the Keio Electronic Laboratory Corporation in Japan. In this respect I do not believe I am putting anything new into the public domain which is not already available on the web somewhere—thanks go to the individuals who have made this material available. (If any individual or corporation has any issue with this, please contact me.)

I am also indebted to a 'Mr Tanaka', whose (Japanese) website got me going in the right direction with respect to the exponential control. Unfortunately his website is no longer extant (though some of it is archived at the [web.archive.org](http://web.archive.org)), which is a shame, as a 'babel fish' translation of his explanation of the reverse saturation mode operation was almost completely incomprehensible to me, as I suspect it was a deal more intuitive than the algebra given here, so it would be nice to see a proper translation of it some day!

## References

- [1] R.M. Kielkowski, *SPICE: Practical Device Modeling*, McGraw-Hill, 1995
- [2] R.M. Kielkowski, *Inside SPICE*, McGraw-Hill, 2<sup>nd</sup> edn., 1998
- [3] R.P. Sallen and E.L. Key, *A Practical Method of Designing RC Active Filters*, IRE Trans. Circuit Theory, Vol. CT-2, pp74–85, March 1955
- [4] R. Schaumann and M.E.van Valkenburg, *Design of Analog Filters*, Oxford University Press 2001
- [5] A.S. Sedra and K.C. Smith, *Microelectronic Circuits*, Oxford University Press, 4<sup>th</sup> edn., 1998
- [6] T.E. Stinchcombe, *Analysis of the Moog Transistor Ladder and Derivative Filters*, 25 Oct 2008, available at:  
[http://www.timstinchcombe.co.uk/synth/Moog\\_ladder\\_tf.pdf](http://www.timstinchcombe.co.uk/synth/Moog_ladder_tf.pdf)
- [7] A. Vladimirescu, *The SPICE Book*, John Wiley & Sons, 1994
- [8] T.H. Wilmshurst, *Analog Circuit Techniques with Digital Interfacing*, Newnes, 2001
- [9] Annual Report, 2000: *Analysis of Student Understanding of Basic AC Concepts*, ONR Research Group, Vanderbilt University,  
<http://www.vuse.vanderbilt.edu/~biswas/Research/ile/onr/year2/index.html>:  
“In our protocols with college professors and field experts alike, we have found that when they come to an obstacle in their reasoning, they resort to equations to solve difficult conceptual problems.”
- [10] LM13700/LM13700A Dual Operational Transconductance Amplifiers with Linearizing Diodes and Buffers, Jun 2004; LM13600 Dual Operational Transconductance Amplifiers with Linearizing Diodes and Buffers, May 1988, National Semiconductor
- [11] ‘SIMetrix AD Plus’ is a mixed-mode simulation package (based on XSpice), produced by SIMetrix Technologies Ltd., Thatcham, Berks (<http://www.simetrix.co.uk/>).